Article

Current Biology

# Evolution of a core ribosomal innovation in octopus

## Graphical abstract

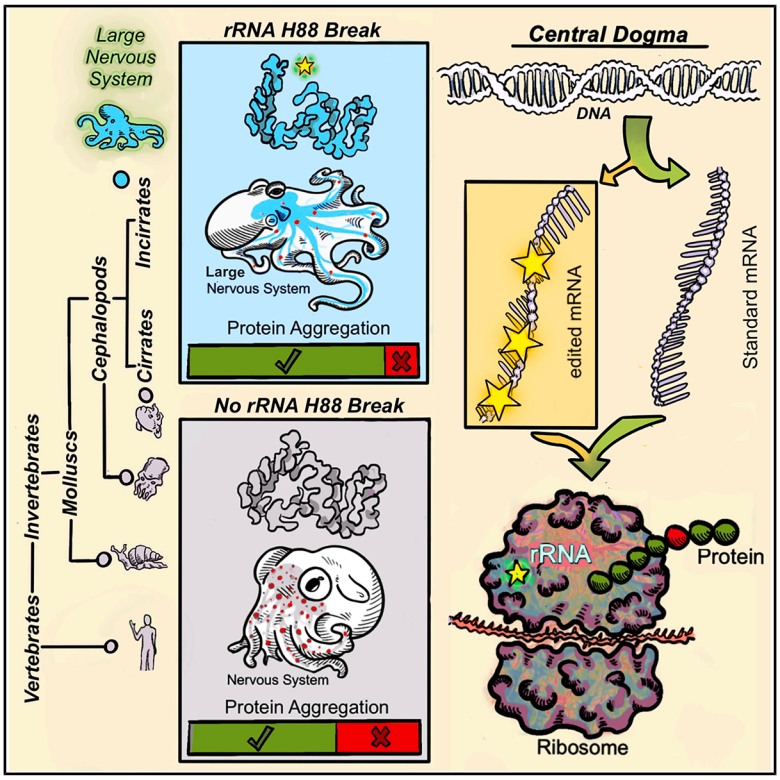


## Highlights

- Octopuses evolved a unique break in the core conserved 28S ribosomal RNA
- The rRNA break enhances translation fidelity and reduces protein aggregation
- Engineering the rRNA break into bacterial ribosomes recapitulates both effects
- The rRNA break evolved in octopuses with expanded nervous systems

## Authors

Rishav Mitra, Richard Han, Trey J. Scott, ..., Michael C. Jewett, Nicholas W. Bellono, Amy S.Y. Lee

## Correspondence

nbellono@harvard.edu (N.W.B.), amysy_lee@dfci.harvard.edu (A.S.Y.L.)

## In brief

Mitra, Han, Scott, et al. discovered a unique structural adaptation in octopus ribosomes that increases the accuracy of protein synthesis and evolved alongside their elaborate nervous systems.

Mitra et al., 2026, Current Biology *36*, 1–10
August 17, 2026 
https://doi.org/10.1016/j.cub.2026.07.008

CellPress

Please cite this article in press as: Mitra et al., Evolution of a core ribosomal innovation in octopus, Current Biology (2026), https://doi.org/10.1016/j.cub.2026.07.008

Current Biology

CellPress

Article

# Evolution of a core ribosomal innovation in octopus

Rishav Mitra,[1,2,3,8] Richard Han,[2,3,8] Trey J. Scott,[1,4,5,8] Anik G. Grearson,[1,2] Jessica A. Willi,[6,7] Christina G. Liu,[1,2,3] Hyeongju Kim,[2,3] Michael C. Jewett,[7] Nicholas W. Bellono,[1,*] and Amy S.Y. Lee[2,3,9,*]

[1]Department of Molecular and Cellular Biology, Harvard University, Cambridge, MA 02138, USA
[2]Department of Cancer Immunology and Virology, Dana-Farber Cancer Institute, Boston, MA 02115, USA
[3]Department of Cell Biology, Harvard Medical School, Boston, MA 02115, USA
[4]Department of Organismic and Evolutionary Biology, Harvard University, Cambridge, MA 02138, USA
[5]Museum of Comparative Zoology, Harvard University, Cambridge, MA 02138, USA
[6]Department of Biochemistry, University of Lethbridge, Lethbridge, AB T1K 3M4, Canada
[7]Chemical and Biological Engineering, Northwestern University, Tech E-135, 2145 Sheridan Road, Evanston, IL 60208, USA
[8]These authors contributed equally
[9]Lead contact
*Correspondence: nbellono@harvard.edu (N.W.B.), amysy_lee@dfci.harvard.edu (A.S.Y.L.)
https://doi.org/10.1016/j.cub.2026.07.008

## SUMMARY

Much of biology focuses on how genetic changes mediate new functions, but less attention is given to adaptations within the ancient molecular machines that execute the central dogma. Octopuses exhibit complex nervous systems and sophisticated behaviors that rival vertebrates but via an entirely divergent evolutionary history. Here, we serendipitously discovered that octopus ribosomes contain a structural break in the core ribosomal RNA that is unique among all animals. This break site enhances translation fidelity to reduce miscoding and subsequent protein aggregation, even when engineered into evolutionarily distant bacterial ribosomes. Furthermore, high-fidelity translation by octopus ribosomes supports proteomic stability during extensive RNA editing observed in cephalopods, suggesting synergy between distinct non-canonical modes of gene regulation. This adaptation emerged in recently derived octopuses with expanded nervous systems, thereby revealing a mechanism that could broadly support the evolution of novel organismal traits.

## INTRODUCTION

Octopuses carry out sophisticated behaviors that are comparable to those of complex vertebrates despite being evolutionarily distant relatives. In contrast to other invertebrates, octopuses exhibit a massively expanded nervous system, with neuron numbers similar to small primates.[1] It remains unclear how such complex adaptations arose over the course of evolution, since octopuses do not exhibit vast genomic novelty when compared with other invertebrates.[2] Post-transcriptional regulation of proteomic diversity has been proposed as a mechanism contributing to the elaboration of the cephalopod nervous system versus those of molluscan relatives[3]; however, mechanisms of protein synthesis in octopus are virtually unexplored.

How do innovations in essential steps of the central dogma downstream of DNA sequence mediate novel functions? Ribosomes are the critical molecular machines that synthesize proteins to form the building blocks of all life.[4] All ribosomes contain a common core of ribosomal RNAs (rRNAs) and proteins that direct protein synthesis. The rRNAs that make up the active sites for tRNA binding, mRNA decoding, and peptide bond catalysis are among the most evolutionarily conserved RNA sequences.[5] Given this universal conservation, structural variation in the core architecture of the ribosome is rarely seen in nature.[6] Therefore, how variations within the ribosome core facilitate changes in the fundamental process of protein synthesis remains poorly understood.

Here, we report the unexpected discovery that octopuses possess structurally unique ribosomes that enhance the accuracy of protein synthesis compared with ribosomes from all other tested animals and in heterologous chimeric systems. Enhanced translation fidelity synergizes with cephalopod-specific RNA hyper-editing to reduce protein aggregation. Furthermore, comparative analyses across octopus suborders and cephalopod relatives reveal that the ribosomal adaptation evolved in the clade of octopuses with expanded nervous systems. Thus, our findings suggest how adaptations within the core translation machinery could help drive the evolution of unique organismal traits and behaviors.

## RESULTS

### The octopus has a unique structural adaptation in the conserved ribosomal core

During routine RNA extraction from octopus tissues (*Octopus bimaculoides*; Figure 1A), we observed that the electrophoretic profile of 28S rRNA was split into distinct fragments (Figure 1B). We further analyzed the rRNA using RT-PCR and rapid amplification of cDNA ends (RACE)-PCR to reveal an octopus-specific sequence "break" localized between nucleotides G4322/C4323 in helix 88 (H88) of the E site (Figure 1C). This was particularly

Please cite this article in press as: Mitra et al., Evolution of a core ribosomal innovation in octopus, Current Biology (2026), https://doi.org/10.1016/j.cub.2026.07.008



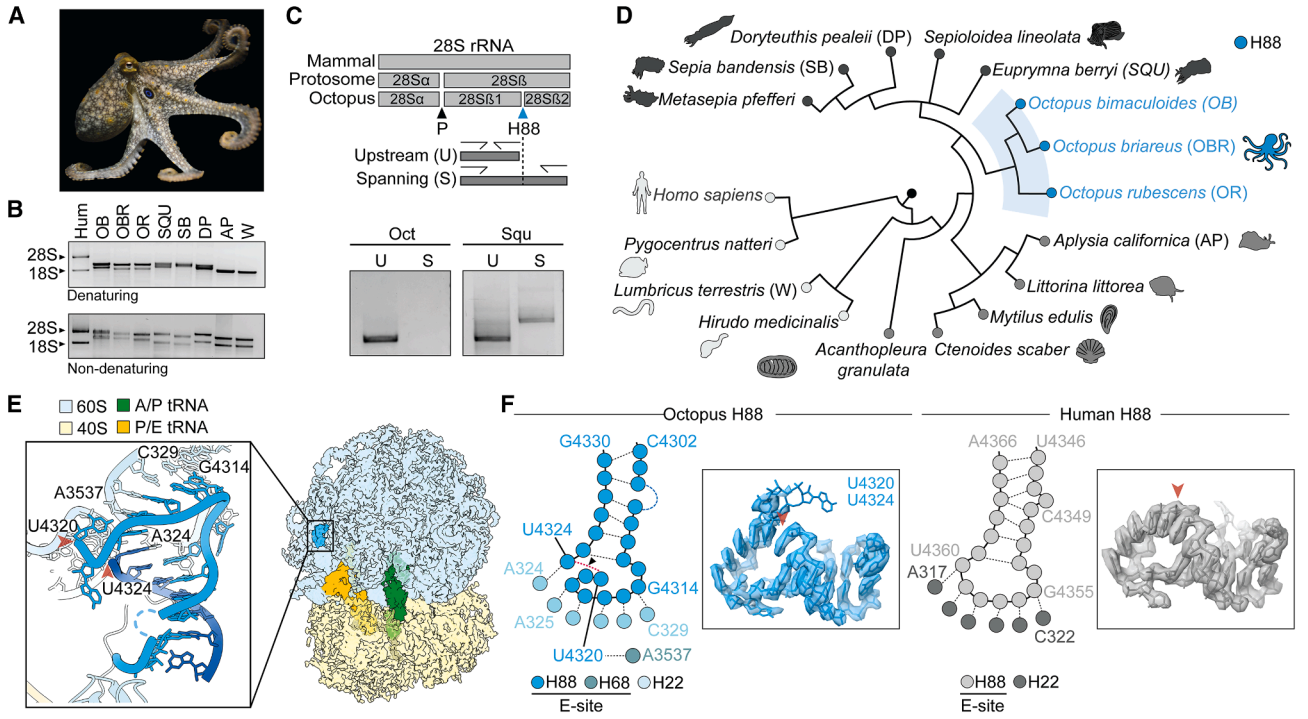


**Figure 1. The octopus has a unique structural adaptation in the conserved ribosomal core**

(A) California two-spot octopus (*Octopus bimaculoides*).

(B) Denaturing and non-denaturing gel electrophoresis of total RNA revealed distinct sizes of rRNA fragments from human (HEK293T cells), *O. bimaculoides* (OB), *Octopus briareus* (OBR), *Octopus rubescens* (OR), *Euprymna berryi* (SQU), *Sepia bandensis* (SB), *Doryteuthis pealeii* (DP), *Aplysia californica* (AP), and *Lumbricus terrestris* (W).

(C) Schematic of the unique octopus 28S rRNA break site in helix 88 (H88) compared with the conserved protostome rRNA gap (P). The octopus break was additionally validated by break-spanning RT-PCR.

(D) Rapid amplification of cDNA ends (RACE)-PCR analysis of RNA isolated from phylogenetically diverse species, including octopuses, cephalopods, mollusks, and others, showed that the H88 break is unique to octopuses.

(E) Cryo-EM structure of octopus ribosome in hybrid-PRE state resolved at 3.2 Å, with H88 highlighted (inset).

(F) Predicted secondary RNA structure of H88 and the cryo-EM structures of octopus and human (PDB: 6OLE[10]) ribosomes, highlighting a loss of electron density and altered base-pairing interactions at the H88 break site. RNA numbering based on NCBI gene entry RNA28SN5.

See also Figures S1–S3 and Table S1.

surprising because this is a highly conserved site in the ribosome that facilitates tRNA exit following peptide bond formation.[7] Notably, this H88 rRNA cleavage is distinct from previously characterized breaks found in the highly variable D6 divergent regions located away from the ribosome catalytic core, such as those observed in protostomes,[8] the naked mole rat,[9] and tuco-tuco[6] (Figure 1C). Sequencing confirmed a contiguous genomic rDNA locus, indicating that the H88 break site originates from a post-transcriptional cleavage event that gives rise to separate rRNA fragments held together through non-covalent interactions (Figures 1B, 1C, and S1A). The break site was only found in octopus and not in any of the other diverse animals we analyzed with RACE-PCR (Figure 1D). Furthermore, it was present across octopus tissues and developmental stages (Figure S1B).

Single-particle cryogenic electron microscopy (cryo-EM) structural analysis determined that the general architecture of the octopus ribosome was conserved compared with other organisms (overall root-mean-square deviation [RMSD] = 1.307 Å; Figures 1E, S2, and S3; Table S1). Consistent with increased flexibility and the presence of an rRNA break, we could not resolve nucleotides 4,321–4,323 and observed a discontinuation in the rRNA density (Figure 1E). Closer investigation of the rRNA revealed additional restructuring of the H88 loop compared with cryo-EM maps of mammalian ribosomes. In both octopus and human ribosomes, nucleotides in the loop of H88 base pair with six nucleotides in helix 22 of the 28S rRNA (octopus 28S rRNA nucleotides 324–329; human 28S rRNA nucleotides 317–322). However, while consecutive bases in the human H88 loop (nucleotides 4,355–4,360) fulfill these interactions, the equivalent base-pairing interactions in the octopus loop are distinct (Figure 1F). On the 5′ side of the break, nucleotides 4,314–4,318 in the H88 loop base pair with nucleotides 329–325 in helix 22, while on the opposite side, only U4324 base pairs with A324. This structural alteration leads to an insertion of five nucleotides surrounding the break site (nucleotides 4,318–4,324), with U4320 stacking with A3537 in helix 68 of 28S rRNA, an interaction not observed in the human ribosome.

## Octopus ribosomes have structural adaptations that facilitate accurate protein synthesis

The ribosomal E site, including helix H88, contacts the 3′ end of deacylated tRNAs and is mechanically coupled to the L1 stalk

Please cite this article in press as: Mitra et al., Evolution of a core ribosomal innovation in octopus, Current Biology (2026), https://doi.org/10.1016/j.cub.2026.07.008



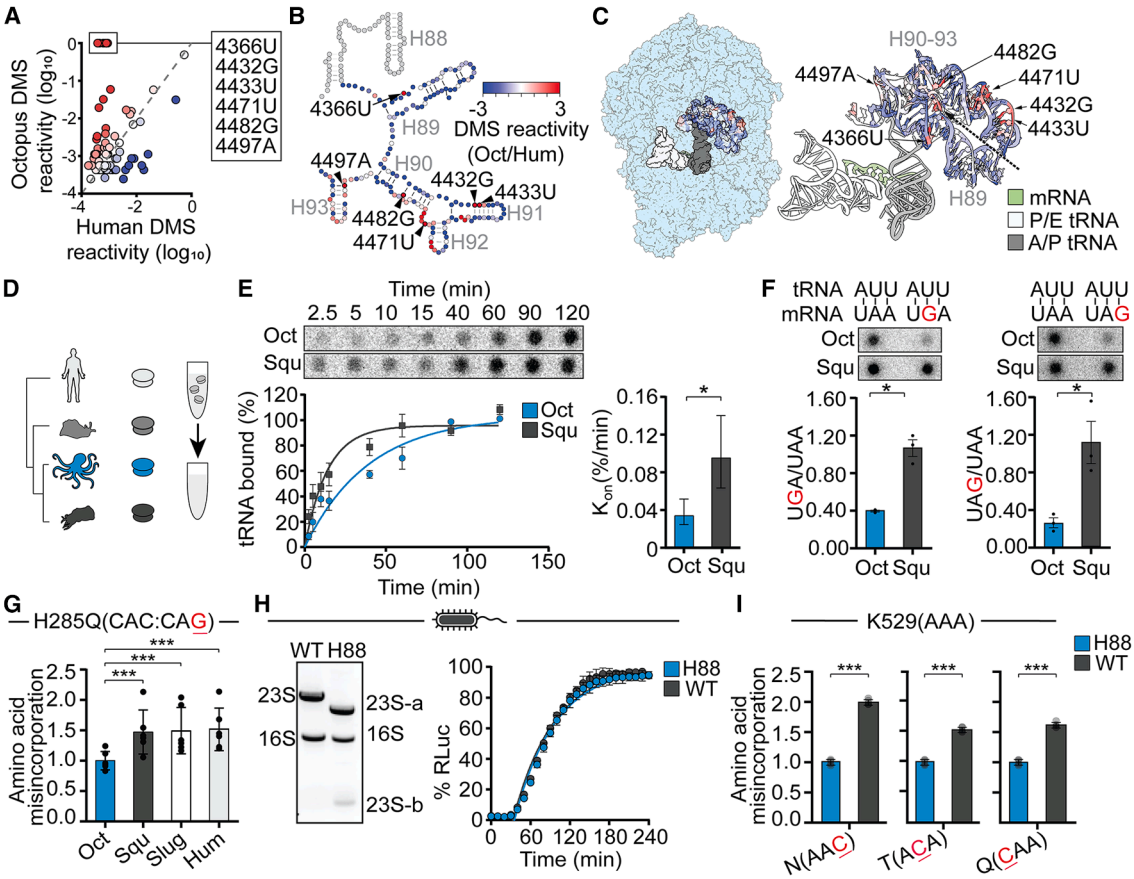


**Figure 2. Octopus ribosomes mediate high-fidelity translation**

(A) Comparative DMS probing of A-site nucleotides across human and octopus ribosomes revealed octopus-specific DMS-hypersensitive sites (4,366U; 4,432G; 4,433U; 4,471U; 4,482G; 4,497A). Residue numbers correspond to the human 60S structure PDB: 6OLE.[10]

(B and C) (B) Nucleotides with increased flexibility in octopus ribosomes cluster in helices H89–93 within the A-site *aa-tRNA* accommodation corridor (black dashed arrow), as shown on the 2D rRNA and (C) 3D ribosome structure (left) with the black dashed rectangle indicating the zoomed-in region of interest (right). Residues have been color mapped as per log2 DMS reactivity (Oct/Hum) according to the scale in (B).

(D) Ribosome-reconstituted *in vitro* reconstitution system to compare ribosomal function across species.

(E) Kinetics of A-site tRNA binding in octopus (Oct) or squid (Squ) ribosomes using radiolabeled ($^{32}$P) suppressor tRNA and ribosome-tRNA filter binding, with first-order rate constants ($n$ = 5).

(F) Octopus ribosomes exhibited more selective mRNA-tRNA pairing compared with squid ribosomes as measured by ribosome-tRNA filter binding using cognate and near-cognate codons ($n$ = 3).

(G) Octopus (Oct) ribosomes exhibited the highest translation fidelity compared with squid (Squ), *Aplysia* (*Slug*), and human (HEK293T; Hum) ribosomes as measured using a luciferase reporter for translation fidelity, where amino acid misincorporation rescues luciferase activity ($n$ = 5).

(H) *E. coli* ribosomes were reconstituted with the octopus H88 break, as shown by denaturing gel electrophoresis of total RNA (left) and *in vitro* translation kinetics (right).

(I) Chimeric ribosomes with the break decrease amino acid misincorporation rates across first, second, and third nucleotide codon positions ($n$ = 6). Data represented as mean ± SEM. *$p$ < 0.05, **$p$ < 0.01, ***$p$ < 0.005 as determined by unpaired Welch's $t$ tests.

See also Figures S3 and S4.

network and subunit movements during translocation and participates in allosteric communication with the decoding center.[11,12] Notably, mutations in the A site (H89–93) that decrease tRNA affinity by increasing local flexibility induce structural changes in H88, suggesting reciprocal communication between the A- and E-site helices.[7,13] In agreement, dimethyl sulfate (DMS) probing revealed heightened reactivity in the A site of the octopus compared with the human ribosome, including in H89 and H91–93, which are part of the aminoacyl-tRNA accommodation corridor and important for selection of the correct tRNA during decoding[14] (Figures 2A–2C). These results indicate that octopus ribosomes exhibit increased A-site flexibility, which could modulate key A-site functions such as tRNA binding.

To ask whether the structural features of the octopus ribosome correspond with functional differences, we developed an *in vitro* translation system that allows reductionist biochemical analyses of ribosomes isolated from non-model organisms. Briefly, we designed a ribosome-reconstitution system using ribosome-depleted rabbit reticulocyte lysates, ribosomes purified from wild-caught animal tissues, and a luciferase mRNA

Please cite this article in press as: Mitra et al., Evolution of a core ribosomal innovation in octopus, Current Biology (2026), https://doi.org/10.1016/j.cub.2026.07.008



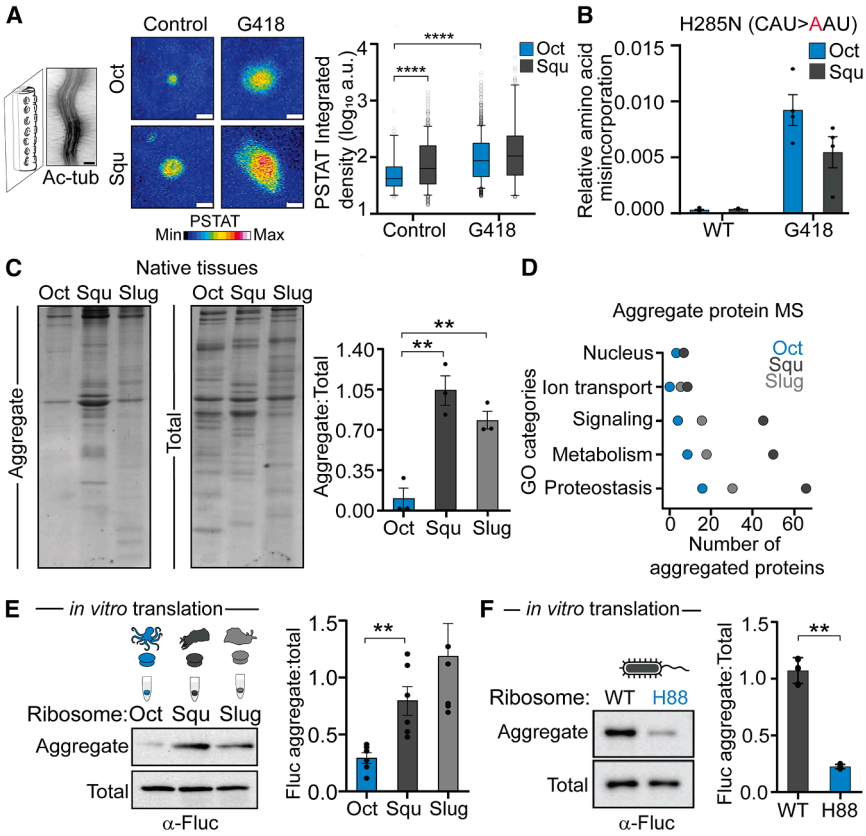


**Figure 3. The H88 ribosomal break facilitates protein synthesis with reduced aggregation**

(A) Octopus axial nerve cords (marked by acetylated α-tubulin; scale bars, 500 μm) had smaller aggresomes compared with squid as visualized by comparative imaging of proteostat (PSTAT)-labeled protein aggresomes, inclusion bodies composed of aggregation-prone proteins. Pharmacological reduction of translation fidelity with G418 increased octopus neuronal aggregation. Scale bars, 1 μm. Data represented as mean ± SEM; $n$ = 4 animals across conditions.

(B) Pharmacological attenuation of translation fidelity with G418 increased misincorporation by octopus to levels comparable to untreated squid as measured using mRNA reporters for translation error ($n$ = 4).

(C) Native tissue insoluble aggregates were lowest in octopus compared with squid and slug, as measured by SDS-PAGE and Coomassie staining of total versus insoluble proteins ($n$ = 3).

(D) Gene Ontology (GO) comparison of aggregated proteins derived from native tissues of octopus (Oct), squid (Squ), or *Aplysia* (Slug) using mass spectrometry showed no preferential enrichment in any particular category.

(E) Octopus ribosomes produced fewer aggregated proteins compared with squid and slug ribosomes as measured by *in vitro* translation of Fluc, aggregated protein separation by centrifugation, and immunoblotting ($n$ = 6).

(F) Chimeric *E. coli* ribosomes with the octopus H88 break produced fewer aggregates when compared with wild-type (WT) ribosomes ($n$ = 3). Data represented as mean ± SEM. $^{*}p < 0.05$, $^{**}p < 0.01$, $^{***}p < 0.005$ as determined by unpaired Welch's $t$ tests.
See also Figure S5.

reporter (Figures 2D, S4A, and S4B). To perform comparative analysis of fundamental translation metrics, we chose the octopus (*O. bimaculoides*) and diverse species without the H88 break, including the squid (*Euprymna berryi*) as another cephalopod, a marine slug (*Aplysia californica*) as a more distantly related mollusk, and human cells (HEK293T). The 28S rRNA across these species exhibits ~90% conservation in the 0.5 kb region flanking the octopus break site.

With this reductionist system, we first used radiolabeled ($^{32}$P) suppressor tRNAs to quantify binding to the A site (Figure S4C). Octopus ribosomes exhibited overall lower tRNA binding affinity and, importantly, a 4-fold reduction in affinity for near-cognate tRNA-mRNA pairing compared with that of squid (Figures 2E and 2F). Thus, octopus ribosomes exhibit increased decoding stringency and favor highly selective mRNA-tRNA pairing. In agreement with the enhanced decoding stringency, we next assessed translation accuracy using a luciferase-based reporter for translation error.[15] Protein synthesis mediated by octopus ribosomes exhibited significantly increased accuracy compared with other species, accompanied by reduced translation efficiency (Figures 2G and S4B).

To test if the octopus H88 break is sufficient to confer enhanced translation fidelity, we used a heterologous *in vitro* reconstituted ribosome-engineering system from *E. coli*.[16] Chimeric *E. coli* ribosomes engineered to contain the octopus H88 rRNA break showed no change in translation efficiency but exhibited a 2-fold increase in fidelity (Figures 2H and 2I). Thus, the octopus-specific H88 ribosome adaptation is sufficient to confer enhanced accuracy of protein synthesis, even when transplanted into evolutionarily distant prokaryotic ribosomes. Notably, engineering similar increases in translation fidelity has broad effects on evolutionary fitness, indicating that the H88 break may represent a beneficial adaptation in octopus.[17] Indeed, the 2-fold change in translation fidelity conferred by the H88 break is comparable to that achieved by ribosomal protein mutations that extend lifespan and stress resistance across diverse species.[18]

## Octopus ribosomes support reduced protein aggregation

What is the cellular impact of enhanced translation fidelity in octopus? Since mistranslation increases protein misfolding and aggregation,[19] we first measured protein aggregation in native octopus tissues. We focused on the nervous system, which is elaborated in octopus and generally enriched in long-lived proteins highly sensitive to translation errors. Under homeostatic conditions, octopus axial nerve cords contained fewer and smaller aggregates compared with squid (Figures 3A and

Please cite this article in press as: Mitra et al., Evolution of a core ribosomal innovation in octopus, Current Biology (2026), https://doi.org/10.1016/j.cub.2026.07.008



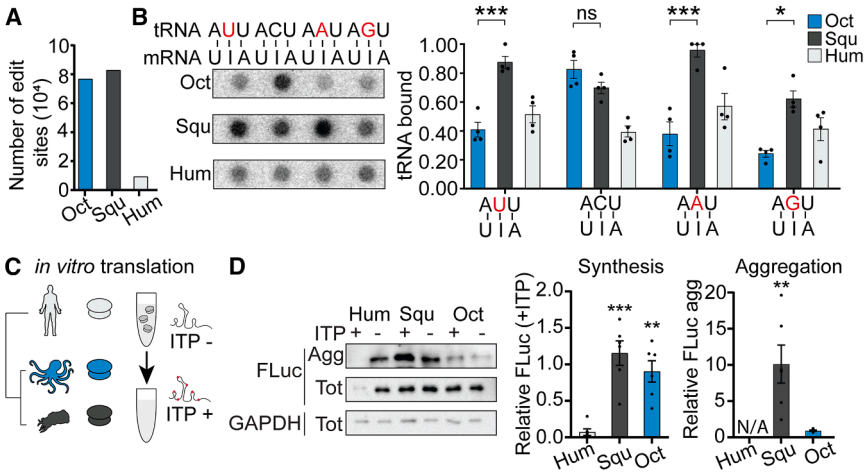


**Figure 4. Octopus ribosomes translate hyper-edited transcripts with reduced aggregation**

(A) Octopus (Oct) and squid (Squ) perform extensive adenosine-to-inosine (A-to-I) RNA editing compared with humans (Hum), at a greater number of editing sites.

(B) Octopus ribosomes selectively decode inosine-containing mRNA codons (strongest I:C pairing), whereas squid ribosomes show promiscuous tRNA binding, as measured by ribosome-tRNA filter binding using an mRNA containing inosine ($n$ = 4). Inosine has the highest binding affinity for cytosine ($\Delta G = -8.8$ kcal/mol) but can also weakly bind adenosine ($\Delta G = -7.5$ kcal/mol), uracil ($\Delta G = -5.9$ kcal/mol), or guanosine ($\Delta G = -6.3$ kcal/mol).[25]

(C and D) Octopus and squid, but not human, ribosomes can translate inosine-containing firefly luciferase (*Fluc*) reporter mRNA. Octopus ribosomes produced fewer aggregated protein than squid ribosomes when translating edited mRNAs. Proteins produced by squid ribosome-mediated translation of edited mRNAs showed 10-fold higher aggregation versus unedited mRNAs (2.6-fold; see Figure 3E), while octopus ribosomes showed no effect of RNA editing on aggregation. ITP = *in vitro* transcribed mRNAs containing inosine ($n$ = 6). Data represented as mean ± SEM; *$p < 0.05$, **$p < 0.01$, ***$p < 0.005$, ****$p < 0.0001$ as determined by unpaired Welch's $t$ tests.

See also Figure S5.

S5B). To examine if this phenotype is sensitive to ribosomal decoding fidelity, we treated *ex vivo* tissue explants with G418, an aminoglycoside antibiotic that induces miscoding by binding to the ribosomal decoding center[20] (Figures 3B and S5A). G418 treatment increased aggregate size in octopus nerve cords and partially reduced the difference in aggregation between species, shifting octopus tissues toward a more squid-like aggregation state (Figure 3B). Thus, the low aggregation state of octopus tissue is sensitive to decoding perturbations, suggesting that ribosomal decoding stringency could contribute to reduced proteotoxic burden. Indeed, insoluble protein aggregates isolated from native tissues across cephalopod relatives and other mollusks demonstrated that octopuses had fewer aggregated proteins across multiple gene families (Figures 3C and 3D).

To directly assess the role of the octopus ribosome in producing fewer protein aggregates, we first measured *in vitro* aggregation of Fluc translated by ribosomes from different species. Translation by octopus ribosomes produced Fluc protein with reduced aggregation propensity compared with squid or slug ribosomes (Figure 3E). Importantly, chimeric *E. coli* ribosomes engineered to contain the octopus H88 rRNA break also generated Fluc protein with lower aggregation compared with protein synthesized by wild-type ribosomes (Figure 3F). Thus, the octopus H88 break directly enhances proteostasis. Consistent with this functional outcome, accurate protein synthesis in octopus is paired with reduced proteasome activity, lower expression of proteostatic machinery, associated signaling pathways, and relaxed evolutionary selection of proteasomal genes (Figures S5C–S5H). Collectively, these findings indicate that octopus ribosomal innovation supports global proteostasis.

## Octopus ribosomes promote accurate decoding of edited RNA

While the central dogma describes the flow of genetic information from DNA to RNA to protein, organisms can bypass this strict conservation of genomic sequence through post-transcriptional modifications that alter mRNAs. In coleoid cephalopods, including octopus and squid, this occurs through a form of post-transcriptional modification called hyperactive adenosine-to-inosine (A-to-I) mRNA editing.[3] RNA editing is particularly prevalent in the expanded cephalopod nervous system, with octopuses containing between 80 and 130,000 sites in protein-coding regions that are subject to adaptive RNA editing and result in recoded proteins[3,21,22] (Figure 4A). However, in other organisms, mRNA editing can lead to nonsynonymous substitutions and misfolding, ribosome stalling, or truncated proteins.[23,24] Considering the octopus ribosome exhibits more stringent mRNA-tRNA pairing (Figure 2E), we hypothesized that this function could facilitate selective decoding of inosine-containing mRNAs.

To characterize how octopus ribosomes interpret edited mRNAs during the decoding process, we examined base-pairing by measuring tRNA binding to mRNAs modified to contain inosine at a single codon position. Consistent with highly selective tRNA pairing, octopus ribosomes showed the highest binding affinity for the most thermodynamically favored inosine-cytosine pair and lower affinity for other promiscuous pairs (Figure 4B). This was in contrast with ribosomes from squid, which exhibited more promiscuous tRNA binding, or human ribosomes, which stall at inosines and cannot translate highly edited mRNA[26] (Figure 4B). Notably, both cephalopod ribosomes were able to translate an inosine-containing FLuc reporter, in contrast to human ribosomes, which likely stall at inosines.[27] Consistent with promiscuous tRNA-mRNA pairing, translation of edited mRNAs by squid ribosomes resulted in a substantial increase in aggregation compared with translation of unedited mRNAs (Figures 3E, 4C, and 4D). However, octopus ribosome-mediated translation resulted in 10-fold lower protein aggregation compared with squid (Figures 4C and 4D). While reduced aggregation of inosine-containing mRNA by octopus ribosomes recapitulates the stringent decoding conferred by the H88 break in heterologous systems (Figure 3F), other native ribosomal properties could

Please cite this article in press as: Mitra et al., Evolution of a core ribosomal innovation in octopus, Current Biology (2026), https://doi.org/10.1016/j.cub.2026.07.008



contribute. Together, these findings suggest that the ability of octopus ribosomes to selectively decode inosine-containing mRNAs could synergize with RNA editing while limiting misfolding and aggregation.

### Evolution of a lineage-specific ribosome innovation

The functional sites (A, P, and E) of the ribosome are highly conserved across all domains of life, and rRNA breaks outside of the octopus are restricted to highly divergent surface-exposed regions away from the core center.[8,9,28] How, then, did the H88 break originate? Octopus and squid are separated by almost 300 million years of evolution.[29] Thus, we sought to analyze the H88 rRNA break across more closely related lineages to understand the evolutionary origins of the break. Octopuses comprise two major suborders: (1) Incirrates, the most prevalent octopuses that live within shallow depths and utilize a highly expanded nervous system to thrive within variable, predator-rich environments using their autonomous sensory arms for hunting, complex camouflage behaviors, and the capacity for learning and rapid decision-making,[30,31] and (2) the understudied and often inaccessible Cirrates, which diverged over 100 million years ago in the Late Cretaceous period[32] and inhabit deep-sea environments with minimal sensory input by using simpler nervous systems to facilitate slow-swimming and passive-feeding lifestyles[33,34] (Figures 5A, 5B, and S6A).

To test whether the H88 rRNA break evolved in concert with nervous system expansion in Incirrates, we analyzed a deep-sea Cirrate (*Grimpoteuthis*) collected at a depth of 406 m via slurp sampling by a remotely operated vehicle (Figure 5C). Strikingly, comparative RT-PCR of RNA extracted from *Grimpoteuthis* tissue demonstrated complete absence of the H88 rRNA break that we observed in every other Incirrate octopus examined (Figures 5D and 1D). To more comprehensively characterize the extent of the H88 rRNA break in cephalopods, we searched for RNA sequence determinants across cephalopods. The rRNA break occurs at a highly conserved region of the large ribosomal subunit that emerged early in ribosomal evolution.[35] Remarkably, the break site corresponds to a specific DNA sequence (TATG/CGTC) that has been perfectly conserved across almost 100 million years of diversification in the Incirrata lineage of cephalopods (Figure 5E). This conserved break site sequence represents a lineage-specific innovation, with Incirrates showing numerous substitutions around the break, despite all other cephalopods and other animals exhibiting high conservation in this region (Figures S6C and S6D). Intriguingly, this divergent evolutionary path is mirrored in the ribosomal break site and in the distinct differences in nervous system expansion across these two clades of octopuses (Figures 5A, 5E, and S6A–S6D).

## DISCUSSION

The ribosome contains highly conserved foundational structures that trace back billions of years, especially within the core rRNA regions that form the A, P, and E sites involved in mRNA decoding and peptide bond synthesis. Here, we show that a naturally occurring rRNA break in the E site of the octopus ribosome modulates central ribosome function to enhance translation fidelity and reduce protein aggregation. Importantly, engineering the octopus rRNA break into a highly divergent prokaryotic ribosome confers higher translation fidelity, highlighting the evolutionary modularity of the ribosome to accommodate adaptations while preserving essential catalytic function. Indeed, single amino acid substitutions in ribosomal proteins distant from the core of the ribosome have been shown to enhance translational fidelity and extend lifespan and stress resistance in yeast, worms, and flies.[18] While octopus ribosomes translate ~30% slower than those from squid or slugs, this property is independent of the H88 break, which is sufficient to enhance fidelity without slowing translation rates in *E. coli*. Thus, the H88 break decouples accuracy gains from canonical speed-fidelity trade-offs. Altogether, these findings suggest that ribosome innovations could support specific organismal demands in a manner that is more widespread than currently appreciated and therefore represents a key aspect of the central dogma to be further explored.

Unlike vertebrates, nervous system expansion in octopuses appears to be driven by ecological rather than social factors,[36] as their sophisticated behaviors evolved in largely solitary and short-lived lifestyles.[37,38] Because Incirrate octopuses require rapid gene expression regulation to survive in a dynamic shallow marine environment, we speculate that high-fidelity translation may have been favored as it supports proteomic flexibility through RNA editing. Squid, lacking this ribosomal innovation, instead evolved hyperactive proteasomes (Figures S5C–S5H), which could mitigate the proteotoxic burden of RNA editing. Altogether, octopuses exhibit innovations across levels of the central dogma. These synergistic adaptations point to a distinct evolutionary strategy that allows for enhanced phenotypic flexibility.

### Limitations of the study

Here, we use *in vitro* biochemistry, reductionist systems, and phylogenetics to reveal how an rRNA break in the octopus ribosome alters ribosome function and proteostasis. However, a limitation of our study is the lack of experimental tools to study octopus protein synthesis *in vivo*, with nearly no protocols established in wild-caught animals outside of this work. Future development of challenging genetics and primary cell culture approaches would allow us to further probe the synergy between ribosome adaptations and gene regulation programs and, ultimately, their relationships to complex animal physiology. Furthermore, direct comparison of ribosomes from Cirrate and Incirrate octopus relatives that differ in natural habitat and presence of the H88 rRNA break would be of great interest; however, obtaining deep-sea Cirrates is extraordinarily difficult and rare. While numerous technical challenges remain, our initial discovery of an innovation within octopus ribosomes establishes powerful conceptual approaches in comparative biochemistry and heterologous systems. Furthermore, the relationship between species-specific ribosomes and organismal behavior provides a foundational blueprint for studying ribosome evolution and function across the diversity of life.

## RESOURCE AVAILABILITY

### Lead contact

Further information and requests for resources and reagents should be directed to and will be fulfilled by the lead contact, Amy S.Y. Lee (amysy_lee@dfci.harvard.edu).

Please cite this article in press as: Mitra et al., Evolution of a core ribosomal innovation in octopus, Current Biology (2026), https://doi.org/10.1016/j.cub.2026.07.008



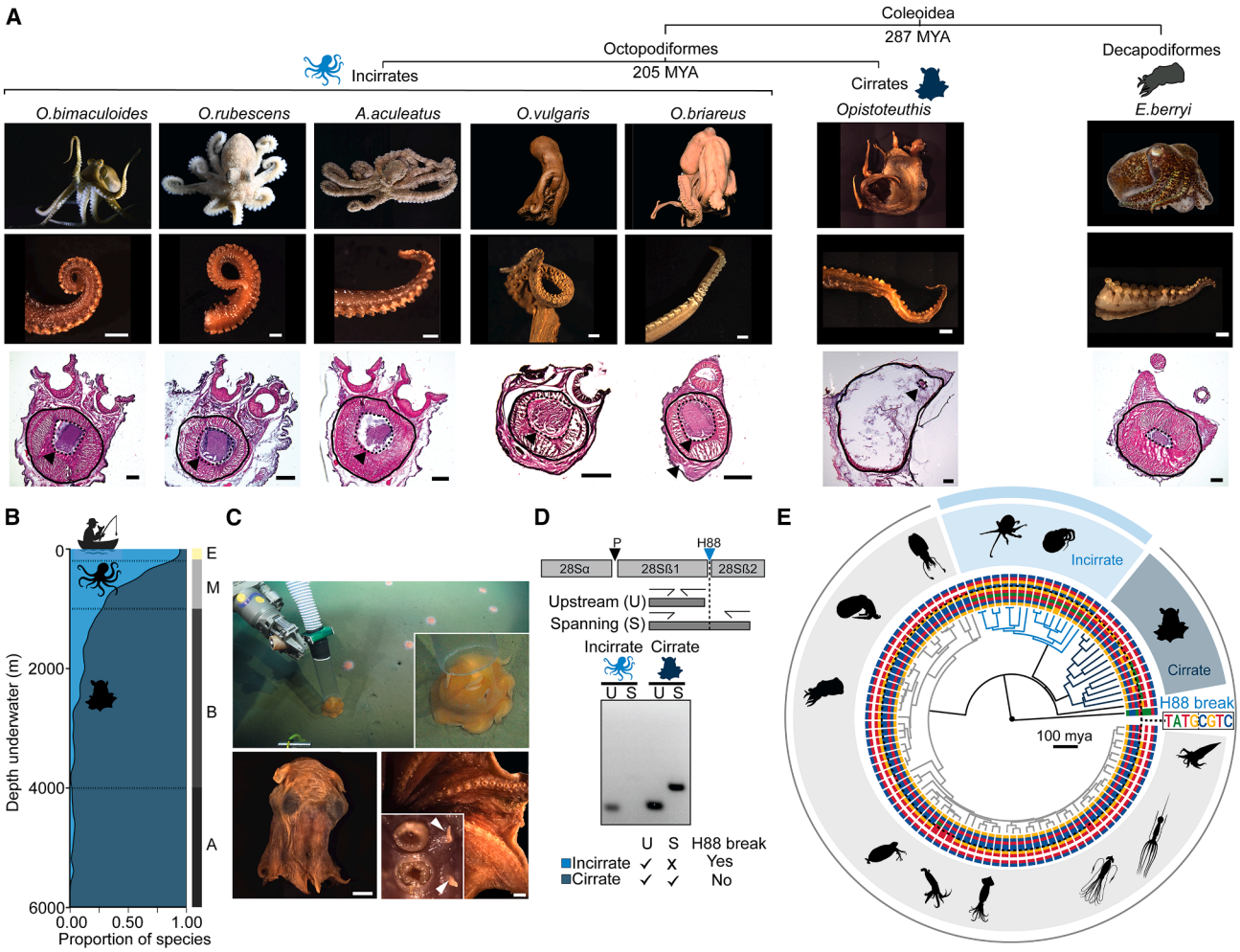


**Figure 5. The octopus H88 break is a lineage-specific innovation that evolved in Incirrate octopuses**

(A) Phylogenetic tree for coleoid cephalopods with comparative arm histology of Incirrate (*Octopus bimaculoides*, *Octopus rubescens*, *Abdopus aculeatus*, *Octopus vulgaris*, and *Octopus briareus*), Cirrate (*Opistoteuthis*), and Decapodiformes (*Euprymna berryi*). Arm cross sections reveal an expanded axial nerve cord in the Incirrates. Scale bars, 1 mm for arm images and 500 μm for arm cross sections.

(B) Depth distributions indicate that Incirrates inhabit shallow waters, while their closest relatives, the Cirrates, are predominantly found in the deep sea. The right bar indicates zone layers of the ocean: E, epipelagic (yellow); M, mesopelagic (light gray); B, bathypelagic (dark gray); A, abyssopelagic (black).

(C) Top: collection of a deep-sea Cirrate octopus (*Grimpoteuthis*) using a remotely operated vehicle (ROV). Bottom: museum specimens of Cirrate octopuses (*Opistoteuthis*). Inset: magnified view of arms and sucker cups. Scale bars (left to right), 1 cm, 500 μm, and 2 mm. White arrows point to the cirri.

(D) rRNA RT-PCR spanning the H88 region reveals that the H88 break site is unique to Incirrates.

(E) The H88 break site is highly conserved in only the Incirrate lineage of octopuses (light blue) but absent in the Cirrates (dark blue) and other cephalopods (gray). Comparative phylogenetic analysis across cephalopods shows that the break sequence is an Incirrate-specific innovation in a region of high genomic conservation.

See also Figures S5 and S6.

## Materials availability

Reagents generated by the authors will be made available to other researchers upon request.

## Data and code availability

- All sequencing data have been deposited in the Gene Expression Omnibus under accession number GEO: GSE284564 and BioProject: PRJNA1199547 and are publicly available as of the date of publication.
- Coordinates and density maps of the octopus ribosome have been deposited in the Protein Data Bank (PDB) under the accession number PDB: 9EHO and the Electron Microscopy Data Bank (EMDB) under the accession numbers EMD-48049, EMD-48050, EMD-48051, and EMD-48061.
- This paper does not report original code.
- Any additional information required to reanalyze the data reported in this paper is available from the lead contact upon request.

## ACKNOWLEDGMENTS

We thank C. Winkler for providing octopuses; B. Grasse of the Cephalopod Program and the Marine Resource Center at the MBL for squid and other invertebrates; B. Walsh and P. Kilian for assistance with animal care and experiments; the Harvard Center for Biological Imaging for imaging and consultation services; the Taplin Mass Spectrometry Facility for proteomics services; J. Gao, M. Yip, S. Shao, the Harvard Center for Cryo-electron Microscopy

(HC2EM), and SBGrid for help with structure determination and analysis; P. Girguis and the Scripps Institution of Oceanography Benthic Invertebrate Collection (SIO-BIC M17639, W7150, M11294, M11232, and M11058); the captain and crew of R/V *Falkor* and the pilots and technicians of ROV *SuBastian* (cruise number FK181005); and members of the Bellono lab, Lee lab, and K. Chat for discussions. L. Soucy is the graphical abstract artist. This research was supported by grants to N.W.B. from the New York Stem Cell Foundation, the Harvard NeuroDiscovery Center, and the National Institutes of Health (R35GM142697); grants to A.S.Y.L. from the Pew Biomedical Scholars Program, the Mathers Foundation, and the National Institutes of Health (R35GM142527); a Harvard Brain Science Initiative (HBI) Postdoctoral Pioneers grant to R.M.; and an NRSA fellowship to R.H. (F31NS132412). T.J.S. is a fellow of the Jane Coffin Childs Fund for Medical Research.

## AUTHOR CONTRIBUTIONS

Conceptualization, A.S.Y.L. and N.W.B.; methodology, R.H., R.M., A.G.G., J.A.W., and C.G.L.; investigation, R.H., R.M., A.G.G., J.A.W., C.G.L., and H.K.; formal analysis, R.M. and T.J.S.; writing – original draft, R.M., A.S.Y.L., and N.W.B.; writing – review & editing, all authors; supervision, A.S.Y.L. and N.W.B.; funding acquisition, A.S.Y.L. and N.W.B.

## DECLARATION OF INTERESTS

The authors declare no competing interests.

## STAR★METHODS

Detailed methods are provided in the online version of this paper and include the following:

- KEY RESOURCES TABLE
- EXPERIMENTAL MODEL AND STUDY PARTICIPANT DETAILS
  - Animal ethics
  - HEK293T cell line
- METHOD DETAILS
  - RNA extraction and gel electrophoresis
  - RACE-PCR
  - Ribosome purification
  - Cryo-EM structure determination
  - DMS probing
  - Ribosome-reconstituted in vitro translation
  - Reconstitution of the H88 break in E. coli ribosomes
  - A-site tRNA filter binding
  - Protein aggregate isolation and quantification
  - Proteasome activity assays
  - Immunohistochemistry
  - *Ex vivo* tissue culture
  - rRNA break analysis RT-PCR
  - RNA sequencing and bioinformatics
  - rDNA phylogenomics
  - Inference of relaxed or intensified selection
  - Octopus depth analysis
- QUANTIFICATION AND STATISTICAL ANALYSIS

## SUPPLEMENTAL INFORMATION

Supplemental information can be found online at https://doi.org/10.1016/j.cub.2026.07.008.

Received: May 22, 2025
Revised: February 27, 2026
Accepted: July 2, 2026

## REFERENCES

1. Deryckere, A., and Seuntjens, E. (2018). The cephalopod large brain enigma: are conserved mechanisms of stem cell expansion the key? Front. Physiol. *9*, 1160. https://doi.org/10.3389/fphys.2018.01160.
2. Albertin, C.B., Simakov, O., Mitros, T., Wang, Z.Y., Pungor, J.R., Edsinger-Gonzales, E., Brenner, S., Ragsdale, C.W., and Rokhsar, D.S. (2015). The octopus genome and the evolution of cephalopod neural and morphological novelties. Nature *524*, 220–224. https://doi.org/10.1038/nature14668.
3. Liscovitch-Brauer, N., Alon, S., Porath, H.T., Elstein, B., Unger, R., Ziv, T., Admon, A., Levanon, E.Y., Rosenthal, J.J.C., and Eisenberg, E. (2017). Trade-off between transcriptome plasticity and genome evolution in cephalopods. Cell *169*, 191–202.e11. https://doi.org/10.1016/j.cell.2017.03.025.
4. Ramakrishnan, V. (2002). Ribosome structure and the mechanism of translation. Cell *108*, 557–572. https://doi.org/10.1016/s0092-8674(02)00619-0.
5. Fox, G.E. (2010). Origin and evolution of the ribosome. Cold Spring Harb. Perspect. Biol. *2*, a003483. https://doi.org/10.1101/cshperspect.a003483.
6. Gutierrez-Vargas, C., De, S., Maji, S., Liu, Z., Ke, Z., Nieß, M., Seluanov, A., Gorbunova, V., and Frank, J. (2026). Structures of naked mole-rat, tuco-tuco, and guinea pig ribosomes-is rRNA fragmentation linked to translational fidelity? Nucleic Acids Res. *54*, gkag006. https://doi.org/10.1093/nar/gkag006.
7. Rakauskaite, R., and Dinman, J.D. (2008). rRNA mutants in the yeast peptidyltransferase center reveal allosteric information networks and mechanisms of drug resistance. Nucleic Acids Res. *36*, 1497–1507. https://doi.org/10.1093/nar/gkm1179.
8. Natsidis, P., Schiffer, P.H., Salvador-Martínez, I., and Telford, M.J. (2019). Computational discovery of hidden breaks in 28S ribosomal RNAs across eukaryotes and consequences for RNA Integrity Numbers. Sci. Rep. *9*, 19477. https://doi.org/10.1038/s41598-019-55573-1.
9. Azpurua, J., Ke, Z., Chen, I.X., Zhang, Q., Ermolenko, D.N., Zhang, Z.D., Gorbunova, V., and Seluanov, A. (2013). Naked mole-rat has increased translational fidelity compared with the mouse, as well as a unique 28S ribosomal RNA cleavage. Proc. Natl. Acad. Sci. USA *110*, 17350–17355. https://doi.org/10.1073/pnas.1313473110.
10. Li, W., Ward, F.R., McClure, K.F., Chang, S.T.L., Montabana, E., Liras, S., Dullea, R.G., and Cate, J.H.D. (2019). Structural basis for selective stalling of human ribosome nascent chain complexes by a drug-like molecule. Nat. Struct. Mol. Biol. *26*, 501–509. https://doi.org/10.1038/s41594-019-0236-8.
11. Mohan, S., and Noller, H.F. (2017). Recurring RNA structural motifs underlie the mechanics of L1 stalk movement. Nat. Commun. *8*, 14285. https://doi.org/10.1038/ncomms14285.
12. Fei, J., Bronson, J.E., Hofman, J.M., Srinivas, R.L., Wiggins, C.H., and Gonzalez, R.L., Jr. (2009). Allosteric collaboration between elongation factor G and the ribosomal L1 stalk directs tRNA movements during translation. Proc. Natl. Acad. Sci. USA *106*, 15702–15707. https://doi.org/10.1073/pnas.0908077106.
13. Rakauskaite, R., and Dinman, J.D. (2011). Mutations of highly conserved bases in the peptidyltransferase center induce compensatory rearrangements in yeast ribosomes. RNA *17*, 855–864. https://doi.org/10.1261/rna.2593211.
14. Sanbonmatsu, K.Y., Joseph, S., and Tung, C.S. (2005). Simulating movement of tRNA into the ribosome during decoding. Proc. Natl. Acad. Sci. USA *102*, 15854–15859. https://doi.org/10.1073/pnas.0503456102.
15. Kramer, E.B., Vallabhaneni, H., Mayer, L.M., and Farabaugh, P.J. (2010). A comprehensive analysis of translational missense errors in the yeast Saccharomyces cerevisiae. RNA *16*, 1797–1808. https://doi.org/10.1261/rna.2201210.
16. Jewett, M.C., Fritz, B.R., Timmerman, L.E., and Church, G.M. (2013). In vitro integration of ribosomal RNA synthesis, ribosome assembly, and translation. Mol. Syst. Biol. *9*, 678. https://doi.org/10.1038/msb.2013.31.

17. Varanda, A.S., Santos, M., Soares, A.R., Vitorino, R., Oliveira, P., Oliveira, C., and Santos, M.A.S. (2020). Human cells adapt to translational errors by modulating protein synthesis rate and protein turnover. RNA Biol. *17*, 135–149. https://doi.org/10.1080/15476286.2019.1670039.

18. Martinez-Miguel, V.E., Lujan, C., Espie-Caullet, T., Martinez-Martinez, D., Moore, S., Backes, C., Gonzalez, S., Galimov, E.R., Brown, A.E.X., Halic, M., et al. (2021). Increased fidelity of protein synthesis extends lifespan. Cell Metab. *33*, 2288–2300.e12. https://doi.org/10.1016/j.cmet.2021.08.017.

19. Drummond, D.A., and Wilke, C.O. (2008). Mistranslation-induced protein misfolding as a dominant constraint on coding-sequence evolution. Cell *134*, 341–352. https://doi.org/10.1016/j.cell.2008.05.042.

20. Wohlgemuth, I., Garofalo, R., Samatova, E., Günenç, A.N., Lenz, C., Urlaub, H., and Rodnina, M.V. (2021). Translation error clusters induced by aminoglycoside antibiotics. Nat. Commun. *12*, 1830. https://doi.org/10.1038/s41467-021-21942-6.

21. Yablonovitch, A.L., Deng, P., Jacobson, D., and Li, J.B. (2017). The evolution and adaptation of A-to-I RNA editing. PLoS Genet. *13*, e1007064. https://doi.org/10.1371/journal.pgen.1007064.

22. Rosenthal, J.J.C., and Eisenberg, E. (2023). Extensive recoding of the neural proteome in cephalopods by RNA editing. Annu. Rev. Anim. Biosci. *11*, 57–75. https://doi.org/10.1146/annurev-animal-060322-114534.

23. Peng, X.X., Xu, X.Y., Wang, Y.M., Hawke, D.H., Yu, S.X., Han, L., Zhou, Z.C., Mojumdar, K., Jeong, K.J., Labrie, M., et al. (2018). A-to-I RNA editing contributes to proteomic diversity in cancer. Cancer Cell *33*, 817–828.e7. https://doi.org/10.1016/j.ccell.2018.03.026.

24. Han, L., Diao, L.X., Yu, S.X., Xu, X.Y., Li, J., Zhang, R., Yang, Y., Werner, H.M.J., Eterovic, A.K., Yuan, Y., et al. (2015). The genomic landscape and clinical relevance of A-to-I RNA editing in human cancers. Cancer Cell *28*, 515–528. https://doi.org/10.1016/j.ccell.2015.08.013.

25. Martin, F.H., Castro, M.M., Aboul-Ela, F., and Tinoco, I., Jr. (1985). Base pairing involving deoxyinosine: implications for probe design. Nucleic Acids Res. *13*, 8927–8938. https://doi.org/10.1093/nar/13.24.8927.

26. Licht, K., Hartl, M., Amman, F., Anrather, D., Janisiw, M.P., and Jantsch, M.F. (2019). Inosine induces context-dependent recoding and translational stalling. Nucleic Acids Res. *47*, 3–14. https://doi.org/10.1093/nar/gky1163.

27. Gupta, R., Kasturi, P., Bracher, A., Loew, C., Zheng, M., Villella, A., Garza, D., Hartl, F.U., and Raychaudhuri, S. (2011). Firefly luciferase mutants as sensors of proteome stress. Nat. Methods *8*, 879–884. https://doi.org/10.1038/nmeth.1697.

28. Melen, G.J., Pesce, C.G., Rossi, M.S., and Kornblihtt, A.R. (1999). Novel processing in a mammalian nuclear 28S pre-rRNA: tissue-specific elimination of an 'intron' bearing a hidden break site. EMBO J. *18*, 3107–3118. https://doi.org/10.1093/emboj/18.11.3107.

29. Chen, Z., Baeza, J.A., Chen, C., Gonzalez, M.T., González, V.L., Greve, C., Kocot, K.M., Arbizu, P.M., Moles, J., Schell, T., et al. (2025). A genome-based phylogeny for Mollusca is concordant with fossils and morphology. Science *387*, 1001–1007. https://doi.org/10.1126/science.ads0215.

30. Bidel, F., Bennett, N.C., and Wardill, T.J. (2022). Octopus bimaculoides' arm recruitment and use during visually evoked prey capture. Curr. Biol. *32*, 4780–4781. https://doi.org/10.1016/j.cub.2022.10.010.

31. Hochner, B. (2012). An embodied view of octopus neurobiology. Curr. Biol. *22*, R887–R892. https://doi.org/10.1016/j.cub.2012.09.001.

32. Tanner, A.R., Fuchs, D., Winkelmann, I.E., Gilbert, M.T.P., Pankey, M.S., Ribeiro, Â.M., Kocot, K.M., Halanych, K.M., Oakley, T.H., da Fonseca, R.R., et al. (2017). Molecular clocks indicate turnover and diversification of modern coleoid cephalopods during the Mesozoic Marine Revolution. Proc. Biol. Sci. *284*, 20162818. https://doi.org/10.1098/rspb.2016.2818.

33. Golikov, A.V., Stauffer, J.B., Schindler, S.V., Taylor, J., Boehringer, L., Purser, A., Sabirov, R.M., and Hoving, H.J. (2023). Miles down for lunch: deep-sea in situ observations of Arctic finned octopods Cirroteuthis muelleri suggest pelagic-benthic feeding migration. Proc. Biol. Sci. *290*, 20230640. https://doi.org/10.1098/rspb.2023.0640.

34. Verhoeff, T.J. (2023). The molecular phylogeny of cirrate octopods (Cephalopoda: Octopoda: Cirrata) using COI and 16S sequences. Folia Malacologica *31*, 175–196. https://doi.org/10.12657/folmal.031.026.

35. Petrov, A.S., Gulen, B., Norris, A.M., Kovacs, N.A., Bernier, C.R., Lanier, K.A., Fox, G.E., Harvey, S.C., Wartell, R.M., Hud, N.V., and Williams, L.D. (2015). History of the ribosome and the origin of translation. Proc. Natl. Acad. Sci. USA *112*, 15396–15401. https://doi.org/10.1073/pnas.1509761112.

36. Chung, W.S., Kurniawan, N.D., and Marshall, N.J. (2022). Comparative brain structure and visual processing in octopus from different habitats. Curr. Biol. *32*, 97–110.e4. https://doi.org/10.1016/j.cub.2021.10.070.

37. Basava, K., Bendixen, T., Leonhard, A., George, N.L., Vanhersecke, Z., Omotosho, J., Mather, J., and Muthukrishna, M. (2026). Ecological not social factors explain brain size in cephalopods: we need a new model for the evolution of big brains. iScience *29*, 116324. https://doi.org/10.1016/j.isci.2026.116324.

38. Basava, K., Bendixen, T., Birk Sørensen, A.L., George, N., Vanhersecke, Z., Omotosho, J., Mather, J., and Muthukrishna, M. (2024). A phylogeny of extant coleoid cephalopods with brain data. Preprint at bioRxiv. https://doi.org/10.1101/2024.04.29.591691.

39. Lee, A.S., Burdeinick-Kerr, R., and Whelan, S.P. (2013). A ribosome-specialized translation initiation pathway is required for cap-dependent translation of vesicular stomatitis virus mRNAs. Proc. Natl. Acad. Sci. USA *110*, 324–329. https://doi.org/10.1073/pnas.1216454109.

40. Lin, Z., Gasic, I., Chandrasekaran, V., Peters, N., Shao, S., Mitchison, T.J., and Hegde, R.S. (2020). TTC5 mediates autoregulation of tubulin via mRNA degradation. Science *367*, 100–104. https://doi.org/10.1126/science.aaz4352.

41. Mukhopadhyay, S., Amodeo, M.E., and Lee, A.S.Y. (2023). eIF3d controls the persistent integrated stress response. Mol. Cell *83*, 3303–3313.e3306. https://doi.org/10.1016/j.molcel.2023.08.008.

42. Lee, A.S., Kranzusch, P.J., and Cate, J.H. (2015). eIF3 targets cell-proliferation messenger RNAs for translational activation or repression. Nature *522*, 111–114. https://doi.org/10.1038/nature14267.

43. Zivanov, J., Nakane, T., Forsberg, B.O., Kimanius, D., Hagen, W.J., Lindahl, E., and Scheres, S.H. (2018). New tools for automated high-resolution cryo-EM structure determination in RELION-3. eLife *7*, e42166. https://doi.org/10.7554/eLife.42166.

44. Rohou, A., and Grigorieff, N. (2015). CTFFIND4: Fast and accurate defocus estimation from electron micrographs. J. Struct. Biol. *192*, 216–221. https://doi.org/10.1016/j.jsb.2015.08.008.

45. Mastronarde, D.N. (2005). Automated electron microscope tomography using robust prediction of specimen movements. J. Struct. Biol. *152*, 36–51. https://doi.org/10.1016/j.jsb.2005.07.007.

46. Pettersen, E.F., Goddard, T.D., Huang, C.C., Meng, E.C., Couch, G.S., Croll, T.I., Morris, J.H., and Ferrin, T.E. (2021). UCSF ChimeraX: Structure visualization for researchers, educators, and developers. Protein Sci. *30*, 70–82. https://doi.org/10.1002/pro.3943.

47. Adams, P.D., Afonine, P.V., Bunkoczi, G., Chen, V.B., Davis, I.W., Echols, N., Headd, J.J., Hung, L.W., Kapral, G.J., Grosse-Kunstleve, R.W., et al. (2010). PHENIX: a comprehensive Python-based system for macromolecular structure solution. Acta Crystallogr. D Biol. Crystallogr. *66*, 213–221. https://doi.org/10.1107/S0907444909052925.

48. Emsley, P., Lohkamp, B., Scott, W.G., and Cowtan, K. (2010). Features and development of Coot. Acta Crystallogr. D Biol. Crystallogr. *66*, 486–501. https://doi.org/10.1107/S0907444910007493.

49. Jamali, K., Kall, L., Zhang, R., Brown, A., Kimanius, D., and Scheres, S.H.W. (2024). Automated model building and protein identification in cryo-EM maps. Nature *628*, 450–457. https://doi.org/10.1038/s41586-024-07215-4.

50. Chen, V.B., Arendall, W.B., 3rd, Headd, J.J., Keedy, D.A., Immormino, R.M., Kapral, G.J., Murray, L.W., Richardson, J.S., and Richardson, D.C. (2010). MolProbity: all-atom structure validation for macromolecular

crystallography. Acta Crystallogr. D Biol. Crystallogr. *66*, 12–21. https://doi.org/10.1107/S0907444909042073.

51. Haas, B.J., Papanicolaou, A., Yassour, M., Grabherr, M., Blood, P.D., Bowden, J., Couger, M.B., Eccles, D., Li, B., Lieber, M., et al. (2013). De novo transcript sequence reconstruction from RNA-seq using the Trinity platform for reference generation and analysis. Nat. Protoc. *8*, 1494–1512. https://doi.org/10.1038/nprot.2013.084.
52. Bray, N.L., Pimentel, H., Melsted, P., and Pachter, L. (2016). Near-optimal probabilistic RNA-seq quantification. Nat. Biotechnol. *34*, 525–527. https://doi.org/10.1038/nbt.3519.
53. Buchfink, B., Xie, C., and Huson, D.H. (2015). Fast and sensitive protein alignment using DIAMOND. Nat. Methods *12*, 59–60. https://doi.org/10.1038/nmeth.3176.
54. Katoh, K., and Standley, D.M. (2013). MAFFT multiple sequence alignment software version 7: improvements in performance and usability. Mol. Biol. Evol. *30*, 772–780. https://doi.org/10.1093/molbev/mst010.
55. Nguyen, L.T., Schmidt, H.A., von Haeseler, A., and Minh, B.Q. (2015). IQ-TREE: a fast and effective stochastic algorithm for estimating maximum-likelihood phylogenies. Mol. Biol. Evol. *32*, 268–274. https://doi.org/10.1093/molbev/msu300.
56. Kalyaanamoorthy, S., Minh, B.Q., Wong, T.K.F., von Haeseler, A., and Jermiin, L.S. (2017). ModelFinder: fast model selection for accurate phylogenetic estimates. Nat. Methods *14*, 587–589. https://doi.org/10.1038/nmeth.4285.
57. Hoang, D.T., Chernomor, O., von Haeseler, A., Minh, B.Q., and Vinh, L.S. (2018). UFBoot2: Improving the Ultrafast Bootstrap Approximation. Mol. Biol. Evol. *35*, 518–522. https://doi.org/10.1093/molbev/msx281.
58. Wertheim, J.O., Murrell, B., Smith, M.D., Kosakovsky Pond, S.L., and Scheffler, K. (2015). RELAX: detecting relaxed selection in a phylogenetic framework. Mol. Biol. Evol. *32*, 820–832. https://doi.org/10.1093/molbev/msu400.
59. Li, W., and Godzik, A. (2006). Cd-hit: a fast program for clustering and comparing large sets of protein or nucleotide sequences. Bioinformatics *22*, 1658–1659. https://doi.org/10.1093/bioinformatics/btl158.
60. Capella-Gutierrez, S., Silla-Martinez, J.M., and Gabaldon, T. (2009). trimAl: a tool for automated alignment trimming in large-scale phylogenetic analyses. Bioinformatics *25*, 1972–1973. https://doi.org/10.1093/bioinformatics/btp348.
61. Cantalapiedra, C.P., Hernandez-Plaza, A., Letunic, I., Bork, P., and Huerta-Cepas, J. (2021). eggNOG-mapper v2: functional annotation, orthology assignments, and domain prediction at the metagenomic scale. Mol. Biol. Evol. *38*, 5825–5829. https://doi.org/10.1093/molbev/msab293.
62. Suyama, M., Torrents, D., and Bork, P. (2006). PAL2NAL: robust conversion of protein sequence alignments into the corresponding codon alignments. Nucleic Acids Res. *34*. W609–612. https://doi.org/10.1093/nar/gkl315.
63. Krueger, F.. Trim Galore: a wrapper tool around Cutadapt and FastQC to consistently apply quality and adapter trimming to FastQ files. https://github.com/FelixKrueger/TrimGalore.
64. Wright, E.S. (2016). Using DECIPHER v2.0 to analyze big biological sequence data in R. R J *8*, 352–359.
65. Telenius, A. (2011). Biodiversity information goes public: GBIF at your service. Nord. J. Bot. *29*, 378–381. https://doi.org/10.1111/j.1756-1051.2011.01167.x.
66. Zhao, C., Liu, F., and Pyle, A.M. (2018). An ultraprocessive, accurate reverse transcriptase encoded by a metazoan group II intron. RNA *24*, 183–195. https://doi.org/10.1261/rna.063479.117.
67. Chandrasekaran, V., Juszkiewicz, S., Choi, J., Puglisi, J.D., Brown, A., Shao, S., Ramakrishnan, V., and Hegde, R.S. (2019). Mechanism of ribosome stalling during translation of a poly(A) tail. Nat. Struct. Mol. Biol. *26*, 1132–1140. https://doi.org/10.1038/s41594-019-0331-x.
68. van Giesen, L., Kilian, P.B., Allard, C.A.H., and Bellono, N.W. (2020). Molecular basis of chemotactile sensation in octopus. Cell *183*, 594–604.e514. https://doi.org/10.1016/j.cell.2020.09.008.
69. Jamali, K., Kall, L., Zhang, R., Brown, A., Kimanius, D., and Scheres, S.H.W. (2023). Automated model building and protein identification in cryo-EM maps. Preprint at bioRxiv. https://doi.org/10.1101/2023.05.16.541002.
70. Lee, A.S., Kranzusch, P.J., Doudna, J.A., and Cate, J.H. (2016). eIF3d is an mRNA cap-binding protein that is required for specialized translation initiation. Nature *536*, 96–99. https://doi.org/10.1038/nature18954.
71. Fritz, B.R., Jamil, O.K., and Jewett, M.C. (2015). Implications of macromolecular crowding and reducing conditions for in vitro ribosome construction. Nucleic Acids Res. *43*, 4774–4784. https://doi.org/10.1093/nar/gkv329.
72. Fritz, B.R., and Jewett, M.C. (2014). The impact of transcriptional tuning on in vitro integrated rRNA transcription and ribosome construction. Nucleic Acids Res. *42*, 6774–6785. https://doi.org/10.1093/nar/gku307.
73. Sakamoto, K., Hayashi, A., Sakamoto, A., Kiga, D., Nakayama, H., Soma, A., Kobayashi, T., Kitabatake, M., Takio, K., Saito, K., et al. (2002). Site-specific incorporation of an unnatural amino acid into proteins in mammalian cells. Nucleic Acids Res. *30*, 4692–4699. https://doi.org/10.1093/nar/gkf589.
74. Yip, M.C.J., Keszei, A.F.A., Feng, Q., Chu, V., McKenna, M.J., and Shao, S. (2019). Mechanism for recycling tRNAs on stalled ribosomes. Nat. Struct. Mol. Biol. *26*, 343–349. https://doi.org/10.1038/s41594-019-0211-4.
75. Planas-Marques, M., Lema, A.S., and Coll, N.S. (2016). Detection and quantification of protein aggregates in plants. Methods Mol. Biol. *1450*, 195–203. https://doi.org/10.1007/978-1-4939-3759-2_15.
76. Altschul, S.F., Gish, W., Miller, W., Myers, E.W., and Lipman, D.J. (1990). Basic local alignment search tool. J. Mol. Biol. *215*, 403–410. https://doi.org/10.1016/S0022-2836(05)80360-2.

Please cite this article in press as: Mitra et al., Evolution of a core ribosomal innovation in octopus, Current Biology (2026), https://doi.org/10.1016/j.cub.2026.07.008





## STAR★METHODS

### KEY RESOURCES TABLE

| REAGENT or RESOURCE | SOURCE | IDENTIFIER |
|---|---|---|
| **Antibodies** | | |
| Mouse monoclonal anti-acetylated tubulin | Sigma | Cat#T6793; RRID: AB_477585 |
| Goat anti-mouse AlexaFluor555 secondary antibody | Invitrogen | Cat#A-21422; RRID: AB_2535844 |
| Rabbit polyclonal anti-firefly luciferase | Proteintech | Cat#27986-AP-1; RRID: AB_2882425 |
| **Bacterial and virus strains** | | |
| *Escherichia coli* BL21 (for TyrRS expression and iSAT ribosome reconstitution; S150/TP70 preparation) | This paper | N/A |
| **Biological samples** | | |
| Octopus bimaculoides (California two-spot octopus); wild-caught adults, aged 1-2 years, male and female | Aquatic Research Consultants | N/A |
| Euprymna berryi (hummingbird bobtail squid); lab-cultured adults, aged 6-8 months | Marine Biological Laboratory, Woods Hole, MA | N/A |
| Aplysia californica (California sea hare); lab-cultured adults, aged 5-8 months | National Resource for Aplysia, Miami, FL | N/A |
| Octopus briareus (Caribbean reef octopus) | Pete's Aquarium, Fishkill, NY | N/A |
| Multiple additional cephalopod, mollusk, and invertebrate species (see method details) | Marine Biological Laboratory, Live Aquaria, Gulf of Maine Inc, Carolina Biological Supply, AquaScapeOnline | N/A |
| Grimpoteuthis sp. (deep-sea Cirrate octopus); collected at 406m depth | ROV SuBastian, cruise FK181005; Scripps Institution of Oceanography Benthic Invertebrate Collection | SIO-BIC M17639, W7150, M11294, M11232, M11058 |
| Rabbit reticulocyte lysate (RRL) | Promega | N/A |
| **Chemicals and recombinant proteins** | | |
| G418 sulfate (aminoglycoside antibiotic) | Fisher Scientific | N/A |
| S-MG132 (proteasome inhibitor) | Cayman Chemical Company | N/A |
| Emetine dihydrochloride (ribosome translocation inhibitor) | Millipore Sigma | Cat#E2375 |
| 4-Benzoyl-L-phenylalanine (Bpa; unnatural amino acid for tRNA charging) | ChemImpex | N/A |
| [alpha-32P]-UTP (radiolabeled nucleotide) | Perkin Elmer | N/A |
| Cycloheximide | Various | N/A |
| Dimethyl sulfate (DMS) | Fisher Scientific | N/A |
| Inosine triphosphate (ITP; for inosine-containing mRNA synthesis) | Various | N/A |
| Recombinant tyrosyl-tRNA synthetase (TyrRS), expressed in E. coli | This paper | N/A |
| Murine RNase inhibitor | NEB | Cat#M0314S |
| Micrococcal nuclease | NEB | N/A |
| Q5 Hot Start DNA polymerase | NEB | Cat#M0491S |
| T7 RNA polymerase (in-house purified) | This paper | N/A |
| **Critical commercial assays** | | |
| Proteostat Aggresome detection kit | Enzo Life Sciences | Cat#ENZ-51035 |

(*Continued on next page*)

Please cite this article in press as: Mitra et al., Evolution of a core ribosomal innovation in octopus, Current Biology (2026), https://doi.org/10.1016/j.cub.2026.07.008



*Continued*

| REAGENT or RESOURCE | SOURCE | IDENTIFIER |
|---|---|---|
| Nile Red staining kit | Abcam | Cat#ab228553 |
| Amytracker630 | Ebba Biotech | N/A |
| Proteasome-Glo Chymotrypsin-Like Cell-Based Assay | Promega | N/A |
| ONE-Glo Luciferase Assay System | Promega | N/A |
| Luciferase assay kit | GeneCopoeia | N/A |
| RNA Clean & Concentrator kit | Zymo Research | N/A |
| RNeasy RNA extraction kit | Qiagen | N/A |
| High-Capacity cDNA Reverse Transcription Kit | Thermo Fisher | N/A |
| Template Switching RT Enzyme Mix | NEB | N/A |
| Poly(A) Polymerase Reaction kit | Thermo Fisher | N/A |
| **Deposited data** | | |
| Cryo-EM density map, empty 80S octopus ribosome | This paper | EMDB: EMD-48049 |
| Cryo-EM density map, 60S ribosomal subunit (multibody refinement) | This paper | EMDB: EMD-48050 |
| Cryo-EM density map, 40S ribosomal subunit (multibody refinement) | This paper | EMDB: EMD-48051 |
| Cryo-EM density map, hybrid 80S octopus ribosome (tRNA-bound state) | This paper | EMDB: EMD-48061 |
| Atomic model coordinates, hybrid 80S octopus ribosome | This paper | PDB: 9EHO |
| RNA sequencing data | This paper | GEO: GSE284564; BioProject: PRJNA1199547 |
| **Experimental models: Cell lines** | | |
| Human: HEK293T | ATCC | Cat#CRL-3216; RRID: CVCL_0063 |
| **Experimental models: Organisms/strains** | | |
| Octopus: Octopus bimaculoides; wild-caught adults | Aquatic Research Consultants | N/A |
| Squid: Euprymna berryi; lab-cultured adults | Marine Biological Laboratory | N/A |
| Sea hare: Aplysia californica; lab-cultured adults | National Resource for Aplysia | N/A |
| Deep-sea octopus: Grimpoteuthis sp. | ROV SuBastian (cruise FK181005) | SIO-BIC collection |
| **Oligonucleotides** | | |
| 3′-RACE anchor primer: 5′-GACCACGCGTATCGATGT CGACTTTTTTTTTTTTTT-3′ | This paper | N/A |
| H88 3′-RACE forward primer: 5′-TGAAAAACCGCCACTTCCGTAGTTTC-3′ | This paper | N/A |
| 3′ RACE reverse primer: 5′-GACCACGCGTATCGATGTCGAC-3′ | This paper | N/A |
| H88 5′-RACE reverse primer: 5′-GCGAGCGCGCAAACCGTTGC-3′ | This paper | N/A |
| Template switching primer (RNA): 5′-GCTAATCATTGCAAGCAGTGGT ATCAACGCAGAGTACATrGrGrG-3′ | This paper | N/A |
| TSO reverse primer: 5′-CATTGCAAGCAGTGGTATCAAC-3′ | This paper | N/A |
| Tyr-ATH-R (shared tRNA primer): 5′-AGTCCGCCGCGTTTAGCCACT-3′ | This paper | N/A |
| Tyr-UUA-ATH-F: 5′-TTAAATCCGCTCCCTTTGGGTTC-3′ | This paper | N/A |
| Tyr-UCA-ATH-F: 5′-TCAAATCCGCTCCCTTTGGGTTC-3′ | This paper | N/A |

(*Continued on next page*)

Please cite this article in press as: Mitra et al., Evolution of a core ribosomal innovation in octopus, Current Biology (2026), https://doi.org/10.1016/j.cub.2026.07.008





*Continued*

| REAGENT or RESOURCE | SOURCE | IDENTIFIER |
|---|---|---|
| Tyr-UGA-ATH-F: 5′-TGAAATCCGCTCCCTTTGGGTTC-3′ | This paper | N/A |
| Tyr-UAA-ATH-F: 5′-TAAAATCCGCTCCCTTTGGGTTC-3′ | This paper | N/A |
| T7-ActB-F: 5'-TAATACGACTCACTATAGGG-3' | This paper | N/A |
| T7-stop-UAG-R: 5′-ACGTGCCTACATGGTGAGCTGG GGGCGGGTGTGG-3′ | This paper | N/A |
| T7-stop-UAA-R: 5′-ACGTGCTTACATGGTGAGCTG GGGGCGGGTGTGG-3′ | This paper | N/A |
| T7-stop-UGA-R: 5′-ACGTGCTCACATGGTGAGCT GGGGGCGGGTGTGG-3′ | This paper | N/A |
| *Grimpoteuthis* H88-spanning F: 5′-AGCTCGCTCGATCTCGATTT-3′ | This paper | N/A |
| *Grimpoteuthis* H88-spanning R: 5′-CCACAAGCCAGTTATCCCTGT-3' | This paper | N/A |
| *Grimpoteuthis* upstream F: 5′-AGCAAAAGGGCAAAAGCTCG-3′ | This paper | N/A |
| *Grimpoteuthis* upstream R: 5′-TGAAAGGATCGATGGGCCAC-3′ | This paper | N/A |
| *O. bimaculoides* H88-spanning F: 5′-AAGGACAAAGCTCGCTCGAT-3′ | This paper | N/A |
| *O. bimaculoides* H88-spanning R: 5′-CAAACGCTTAGCCGTCACAA-3′ | This paper | N/A |
| *O. bimaculoides* upstream F: 5′-AGCTCGCTCGATCACGATTT-3' | This paper | N/A |
| *O. bimaculoides* upstream R: 5′-TTCGGAAAGGATCGATGGGC-3′ | This paper | N/A |
| DMS pair 1 F: 5′-AGCTTGACTCTAGTCTGGCACG-3′ | This paper | N/A |
| DMS pair 1 R: 5′-ACTGACCCGGTGAGGCG-3′ | This paper | N/A |
| DMS pair 2 F: 5′-GTCAAACGGTAACGCAGGTGT-3′ | This paper | N/A |
| DMS pair 2 R: 5′-GCCTCACGATCCTTCTGACCTT-3′ | This paper | N/A |
| DMS pair 3 F: 5′-AATTCACCAAGCGTTGGATTGTTCAC-3′ | This paper | N/A |
| DMS pair 3 R: 5′-TGGTGTATGTGCTTGGC TGAGGA-3′ | This paper | N/A |
| DMS pair 4 F: 5′-GCGCCAGAAGCGAGAGC-3′ | This paper | N/A |
| DMS pair 4 R: 5′-AGGTTTCTGTCCTCCCTGAGC-3′ | This paper | N/A |
| DMS pair 5 F: 5′-CTGACACCTCCTGCT TAAAACCCA-3′ | This paper | N/A |
| DMS pair 5 R: 5′-GCTCACGTTCCCTATTAGTGGGT-3′ | This paper | N/A |
| DMS pair 6 F: 5′-AGATGGTAGCTTCGCCCCATT-3′ | This paper | N/A |
| DMS pair 6 R: 5′-TCCCGCGCGCG-3′ | This paper | N/A |
| **Recombinant DNA** | | |
| pFR-CrPV-RLuc (Renilla luciferase fidelity reporter with CrPV IRES) | Lee et al.[39] | N/A |
| pFR-CrPV-RLuc K529 fidelity mutant (missense mutation at K529 in luciferase catalytic site) | This paper | N/A |
| pk7-Luc (firefly luciferase iSAT reporter, wild-type) | Jewett et al.[16] | N/A |
| pk7-Luc K529 fidelity mutant (iSAT fidelity reporter) | This paper | N/A |
| pT7rrn (E. coli rRNA for iSAT reconstitution, wild-type) | Jewett et al.[16] | N/A |
| pT7rrn H88 mutant (E. coli rRNA with octopus H88 break inserted) | This paper | N/A |

(*Continued on next page*)

Please cite this article in press as: Mitra et al., Evolution of a core ribosomal innovation in octopus, Current Biology (2026), https://doi.org/10.1016/j.cub.2026.07.008



*Continued*

| REAGENT or RESOURCE | SOURCE | IDENTIFIER |
|---|---|---|
| BsT-TyrCUA (B. stearothermophilus amber suppressor tRNA template) | Lin et al.[40] | N/A |
| pcDNA4 Rluc (Renilla luciferase expression vector) | Mukhopadhyay et al.[41] | N/A |
| pcDNA4 PSMB6 5' UTR FLuc (firefly luciferase aggregation reporter) | Lee et al.[42] | N/A |
| pcDNA4 CrPV IRES HA-FLuc (inosine aggregation reporter) | This paper | N/A |
| MarathonRT (reverse transcriptase) | Addgene | Addgene: #109029 |
| **Software and algorithms** | | |
| RELION v3.1 (cryo-EM data processing) | Zivanov et al.[43] | https://relion.readthedocs.io; RRID: SCR_016274 |
| CTFFIND-4.1 (CTF estimation) | Rohou and Grigorieff[44] | https://grigoriefflab.umassmed.edu/ctffind4; RRID: SCR_016732 |
| SerialEM v4.0.5 (cryo-EM data collection) | Mastronarde[45] | https://bio3d.colorado.edu/SerialEM; RRID: SCR_017293 |
| UCSF ChimeraX v1.3-1.6 (structure visualization and rigid body fitting) | Pettersen et al.[46] | https://www.cgl.ucsf.edu/chimerax; RRID: SCR_015872 |
| PHENIX v1.20.1 (real-space refinement) | Adams et al.[47] | https://phenix-online.org; RRID: SCR_014224 |
| Coot v0.9.6 (manual model building) | Emsley et al.[48] | https://www2.mrc-lmb.cam.ac.uk/personal/pemsley/coot; RRID: SCR_014222 |
| ModelAngelo (automated model building in cryo-EM maps) | Jamali et al.[49] | https://github.com/3dem/model-angelo |
| MolProbity (model validation) | Chen et al.[50] | http://molprobity.biochem.duke.edu; RRID: SCR_014226 |
| PyMOL v2.5.3 (structural visualization) | Schrodinger LLC | https://pymol.org; RRID: SCR_000305 |
| GraphPad Prism (statistical analysis and graphing) | GraphPad Software | https://www.graphpad.com; RRID: SCR_002798 |
| ImageLab (gel band intensity quantification) | BioRad | https://www.bio-rad.com; RRID: SCR_014210 |
| Trinity (de novo transcriptome assembly) | Haas et al.[51] | https://github.com/trinityrnaseq; RRID: SCR_013048 |
| Kallisto (RNA-seq quantification) | Bray et al.[52] | https://pachterlab.github.io/kallisto; RRID: SCR_016582 |
| DIAMOND (protein sequence alignment) | Buchfink et al.[53] | https://github.com/bbuchfink/diamond; RRID: SCR_016071 |
| MAFFT v7.490 (multiple sequence alignment) | Katoh and Standley[54] | https://mafft.cbrc.jp/alignment/software; RRID: SCR_011811 |
| IQ-TREE (phylogenetic tree construction) | Nguyen et al.[55] | http://www.iqtree.org; RRID: SCR_017254 |
| ModelFinder (model selection for phylogenetics) | Kalyaanamoorthy et al.[56] | https://www.iqtree.org |
| UFBoot2 (ultrafast bootstrap for phylogenetics) | Hoang et al.[57] | https://www.iqtree.org |
| RELAX (test for relaxed/intensified selection) | Wertheim et al.[58] | http://www.hyphy.org |
| cd-hit (sequence clustering) | Li and Godzik[59] | https://sites.google.com/view/cd-hit; RRID: SCR_007105 |
| trimAl (alignment trimming) | Capella-Gutierrez et al.[60] | http://trimal.cgenomics.org; RRID: SCR_017452 |
| eggNOG-mapper v2 (functional annotation) | Cantalapiedra et al.[61] | https://github.com/eggnogdb/eggnog-mapper; RRID: SCR_021166 |
| PAL2NAL (protein to codon alignment) | Suyama et al.[62] | http://www.bork.embl.de/pal2nal; RRID: SCR_014932 |

(*Continued on next page*)

*Continued*

| REAGENT or RESOURCE | SOURCE | IDENTIFIER |
|---|---|---|
| Trim Galore (quality trimming of RNA-seq reads) | Krueger[63] | https://www.bioinformatics.babraham.ac.uk/projects/trim_galore; RRID: SCR_011847 |
| DECIPHER (consensus rDNA sequence generation) | Wright[64] | https://bioconductor.org/packages/DECIPHER |
| GBIF (species distribution data) | Telenius[65] | https://www.gbif.org |
| Other | | |
| Talos Arctica TEM operating at 200 kV (cryo-EM data collection) | Thermo Fisher Scientific | N/A |
| K3 summit direct electron detector | Gatan | N/A |
| Vitrobot Mark IV (vitrification) | Thermo Fisher Scientific | N/A |
| Q700 sonicator | QSonica | N/A |

## EXPERIMENTAL MODEL AND STUDY PARTICIPANT DETAILS

California two-spot octopuses (*Octopus bimaculoides*) were wild-caught male and female adults (aged 1–2 years, Aquatic Research Consultants) and fed a daily diet of fiddler crabs (Leptuca pugilator, Northeast Brine Shrimp, Oak Hill, FL). All housed animals were kept under a 12 h–12 h light/dark cycle in filtered natural seawater. The influence of sex on the results was not systematically evaluated given that this study focused on ribosome biochemistry across tissues, rather than sex-dependent physiological traits. Adult *Euprymna berryi* (aged 6–8 months) hummingbird bobtail squid (E. berryi) were laboratory cultured at the Marine Biological Laboratory, Woods Hole, MA, and fed daily with grass shrimp (Palaemonetes pugio, Aquatic Indicators). All cephalopods were euthanized using established methods with sedation in 15% ethanol followed by pithing for tissue harvesting. Adult *Aplysia californica* (aged 5–8 months) California sea hares (A. californica) were laboratory cultured (National Resource for Aplysia, Miami, FL), anesthetized in 5–10 animal volumes of 1:1 seawater:isotonic MgCl2, and dissected upon arrival at Harvard University. A deep-sea Cirrate octopus (Grimpoteuthis sp.) was collected at a depth of 406m via slurp-sampling by remotely operated vehicle (ROV SuBastian, cruise FK181005, R/V Falkor). Tissue fragments were collected in 95% ethanol and stored in 50% ethanol until processing. Voucher specimens are deposited at the Scripps Institution of Oceanography Benthic Invertebrate Collection (SIO-BIC M17639, W7150, M11294, M11232, M11058).Tissues for RACE-PCR analyses were obtained from Caribbean reef octopus (Octopus briareus; Pete's Aquarium), Ruby octopus (Octopus rubescens; TONMO), Pyjama squid (Sepioloidea lineolata), Longfin squid (Doryteuthis pealeii), Stumpy cuttlefish (Sepia bandensis), Flamboyant cuttlefish (Metasepia pfefferi) (all from Marine Biological Laboratory, Woods Hole, MA), Flame scallop (Ctenoides scaber), Periwinkle snail (Littorina littorea) (Live Aquaria), Blue mussel (Mytilus edulis), Chiton (Chaetopleura apiculate) (Gulf of Maine Inc.), Leech (Hirudo medicinalis), Earthworm (Lumbricus terrestris) (Carolina Biological Supply), Red-bellied piranha (Pygocentrus nattereri, euthanized in 100 mg $L^{-1}$ MS-222; AquaScapeOnline). All animals were euthanized and harvested for tissues upon arrival at Harvard University.

### Animal ethics

Animal protocols were approved by the Harvard University Animal Care and Use Committee (protocol ID 18-05-325 and 18-05-324) with further guidance from the Marine Biological Laboratory Marine Resources Center.

### HEK293T cell line

Human HEK293T cells (ATCC CRL-3216) were used for DMS probing experiments and ribosome purification as described in method details.

## METHOD DETAILS

### RNA extraction and gel electrophoresis

Tissue was flash-frozen in liquid nitrogen immediately after collection and ground into a fine powder using a mortar and pestle. RNA extraction under denaturing conditions was performed by mixing frozen tissue powder with 10× volume TRIzol (Invitrogen) and isolating the RNA aqueous phase according to the manufacturer's protocol. RNA was further purified using an RNA Clean & Concentrator kit (Zymo). RNA extraction under non-denaturing conditions was performed via phenol-chloroform purification. Tissue powder was resuspended in 3× volume lysis buffer (50 mM Tris-HCl pH 7.5, 10 mM MgCl2, 100 mM 2-mercaptoethanol, 0.5% NP-40 (v/v)), triturated through an 18-g needle, incubated on ice for 10 min, and nuclei were pelleted by spinning at 11,500 × g for 10 min at 4 °C. Total RNA was then purified from lysates by phenol-chloroform extraction and ethanol precipitation and RNA was resuspended in non-denaturing resuspension buffer (10 mM Tris-HCl pH 7.5, 150 mM NaCl, 5 mM MgCl2, 1 mM EDTA-NaOH pH 8). For denaturing RNA gel electrophoresis, RNA was mixed with an equal volume of 2× stop solution (95% deionized formamide, 20 mM EDTA-NaOH

pH 8), incubated at 95 °C for 5 min, and analyzed on 1% (w/v) agarose gels prestained with 2% (w/v) ethidium bromide. For non-denaturing RNA gel electrophoresis, RNA was mixed with 6× non-denaturing loading dye (40% w/v sucrose, with bromophenol blue) and analyzed on 1% (w/v) agarose gels prestained with 2% (w/v) ethidium bromide.

## RACE-PCR

For 3′ RACE-PCR analysis, RNAs were polyadenylated by incubating 5 μg of total RNA in a 25 μL reaction containing 10 mM ATP, 40 U $mL^{-1}$ yeast poly-A polymerase (Thermo Fisher), 1× Poly(A) Polymerase Reaction Buffer (Thermo Fisher), and 25 mM MnCl2 for 10 min at 37 °C. RNA was isolated using an RNA Clean & Concentrator kit (Zymo) and cDNA was generated using Marathon RT (Addgene #109029) and a 3′-RACE-anchor primer (5′-GACCACGCGTATCGATGTCGACTTTTTTTTTTTTTTT-3′) under standard conditions.[66] PCR was subsequently performed using Q5 polymerase (NEB) and H88-3′-RACE-F (5′-TGAAAAACCGCCACTTCCG TAGTTTC-3′) and 3′ RACE-R (5′-GACCACGCGTATCGATGTCGAC-3′) primers under standard conditions. Products were gel extracted and used as template for a second round of PCR amplification. PCR products were inserted into pMiniT 2.0 by PCR cloning (NEB) and the 3′ end of the rRNA was identified by Sanger sequencing. For 5′ RACE-PCR analysis, 3 μg total RNA was annealed with random hexamers as the reverse transcriptase (RT) primer. RT and template switching was performed using the Template Switching RT Enzyme Mix (NEB) and a template switching primer (5′-GCTAATCATTGCAAGCAGTGGTATCAACGCAGAGTACATrGrGrG-3′) according to manufacturer's protocol. PCR was subsequently performed using Q5 polymerase and TSO-R (5′-CATTGCAAGCAGTGG TATCAAC-3′) and the H88-5′-RACE-R (5′-GCGAGCGCGCAAACCGTTGC-3′) primers. PCR products were gel extracted, re-amplified, cloned into vectors, and sequenced as described above.

## Ribosome purification

Ribosomes were isolated from flash-frozen ground tissue powder from *O. bimaculoides* arms, *E. berryi* arms, and *Aplysia* parapodia. Tissue powder was homogenized in lysis buffer (320 mM sucrose, 50 mM Tris-HCl pH 7.5, 100 mM KCl, 10 mM MgCl2, 10 mM DTT, 10 U $mL^{-1}$ murine RNase inhibitor (NEB), 0.1% (v/v) Triton-X 100) and triturated sequentially through a 16-g, 18-g, and 21-g needle. Insoluble material was pelleted by spinning 13,500 × g for 10 min at 4 °C. Lysates were loaded onto a 50% (w/v) sucrose cushion made in lysis buffer without detergent for 18 h at 4 °C at 30,000 rpm in a Type 70.1 Ti rotor. Pelleted ribosomes were resuspended in storage buffer (6% (w/v) sucrose, 100 mM KOAc, 5 mM MgCl2, 30 mM HEPES-KOH pH 7.5, 2 mM DTT), and further purified by centrifugation through S-400 resin for 2 min at 4 °C at 700 × g.[10]

## Cryo-EM structure determination

80S ribosomes were isolated for cryo-EM from octopus arm tissue as described above, but with 10 μM emetine added to the lysis and sucrose cushion buffers. 3 μL of purified octopus monosomes at ~140 nM were applied to glow-discharged R2/2 Cu 300 mesh grids (Quantifoil) covered with a 5 nm layer of continuous carbon and vitrified using a Vitrobot Mark IV (Thermo Fisher Scientific) set at 4 °C and 100% humidity with a wait time of 30 sec, a blot time of 3 sec, and a blot force of +8. Grids were imaged on a Talos Arctica TEM (Thermo Fisher Scientific) operating at 200 kV equipped with a K3 summit direct electron detector (Gatan) in counting mode at a nominal magnification of 36,000× corresponding to a calibrated pixel size of 1.1 Å. Semi-automated data collection was performed using SerialEM v4.0.5. A total exposure time of 4.5 s, corresponding to a total dose of 53 electrons/Å2, was fractionated over 50 frames. The defocus range was −1.5 to −2.5 μm.

988 movies were subjected to motion correction and CTF estimation using CTFFIND-4.1[44] in RELION-3.1,[43] followed by template-free Laplacian-of-Gaussian (LoG)-based automatic particle picking. Following 2D classification, 113,630 particles were subjected to 3D auto-refinement using a 60 Å low-passed initial volume of a rabbit 80S ribosome and 3D classification with 6 classes. 69,888 particles in classes corresponding to 80S ribosomes were subjected to Bayesian polishing and another round of 3D auto-refinement. This dataset was then either directly subjected to multibody refinement of the 60S and 40S ribosomal subunits or to signal subtraction and focused 3D classification without alignments into 6 classes using a mask covering the tRNA binding sites at the ribosomal subunit interface. 15,061 particles corresponding to 80S ribosomes containing hybrid tRNAs and 31,629 particles corresponding to empty 80S ribosomes were separately subjected to a final round of 3D auto-refinement and post-processing in RELION.

The 60S and 40S rabbit ribosomal subunits of PDB:6SGC[67] were separately fitted as rigid bodies into the maps generated from multibody refinement in ChimeraX v1.3.[46] One round of Phenix v1.20.1 real space refinement[47] with only rigid body fitting enabled was performed, and the two ribosomal subunits were initially modelled separately in Coot v0.9.6[48] using the maps generated from multibody refinement. Protein and rRNA sequences were changed to octopus sequences assembled from available annotations and RNA sequencing data (BioProject: PRJNA658966[68]). Where needed, outputs from ModelAngelo[49,69] were used to inform rRNA paths. Several rounds of Phenix v1.20.1 real space refine and manual modelling in Coot were performed before the two ribosomal subunits were rigid body fitted into the map of the empty 80S octopus ribosome in ChimeraX v1.3. Cycloheximide was added manually in Coot v.0.9.6 followed by multiple rounds of manual adjustments in Coot and Phenix v.1.20.1 real space refine. The empty 80S octopus ribosome model was then used as a starting model for the hybrid 80S octopus ribosome. tRNAs were added in Coot based on initial models from PDB: 6SGC, followed by multiple rounds of manual adjustments in Coot and Phenix 1.20.1 real space refine. Model validations were performed with MolProbity[50] in Phenix. Structural interpretations and comparisons were done in Coot v0.9.6, PyMOL v2.5.3, and ChimeraX v1.5 or v1.6. Figure panels were made with ChimeraX v1.5 and v1.6. rRNA structural and sequence comparisons with human ribosomes were performed using PDB: 6Y57 or PDB: 6OLE and NCBI gene entry RNA28SN5.

Please cite this article in press as: Mitra et al., Evolution of a core ribosomal innovation in octopus, Current Biology (2026), https://doi.org/10.1016/j.cub.2026.07.008





### DMS probing

Endogenous ribosomes were purified from human (HEK293T) cells or octopus arm tissue by centrifugation of cell lysate on a sucrose cushion for 20 h at 30,000 rpm using a TLA70.1 rotor. The pelleted ribosomes were resuspended and washed through a high salt cushion (50% (w/v) sucrose, 50 mM Tris-HCl pH 7.5, 10 mM MgCl2, 0.1% (v/v) Triton-X 100, 500 mM KCl) to remove tRNAs by centrifugation for 20 h at 4 °C at 39,000 rpm in a TLA1001.1 rotor. Purified ribosomes were incubated with vehicle (ethanol) or 0.1% of DMS (Fisher scientific) for 30 min, followed by rRNA extraction using TRIzol (Invitrogen) according to the manufacturer's protocol. Purified rRNA was reverse transcribed using MarathonRT (in-house purified from Addgene #109029), followed by cDNA precipitation and purification. Amplicon sequencing was performed with the following primer pairs tiling H89-H93 (sequences listed in key resources table).

### Ribosome-reconstituted in vitro translation

To generate mutant Renilla luciferase plasmids for translation error experiments, the pFR-CrPV-RLuc plasmid,[39] which contains the cricket paralysis virus (CrPV) IRES followed by Renilla luciferase, was prepared by digestion with PciI and XbaI, followed by two-insert Gibson cloning to introduce the mutated sequence. RNAs for luciferase reporter assays were transcribed using T7 RNA polymerase using a purified PCR product as template.[70]

Endogenous ribosomes were pelleted from rabbit reticulocyte lysate (RRL, Promega) by centrifugation for 4 h at 4 °C at 100,000 rpm in a TLA 100.4 rotor. Ribosome-depleted in vitro translation extracts were collected, flash-frozen in single use aliquots, and stored at −80 °C. Before addition to in vitro translation extracts, ribosomes were treated with 4 U $\mu L^{-1}$ micrococcal nuclease (NEB) to digest endogenous ribosome-bound mRNAs. For in vitro translation, each reaction contained 55% (v/v) ribosome-free RRL and 1 μg in vitro transcribed mRNA in a final reaction containing 40 nM purified ribosomes, 20 μM amino acids (Promega), and 1.27 U $\mu L^{-1}$ murine RNase inhibitor (NEB). G418 was added to a final concentration of 70 μg $mL^{-1}$ as indicated. Translation reactions were incubated for 2 h at 30 °C, luciferase assay was performed (GeneCopoeia), and relative luminescence units were measured using a Glomax Multi+ plate reader (Promega). For measuring translation fidelity, in vitro translation was performed in paired assays using WT or mutant luciferase mRNA. Point mutations are in the catalytic site of luciferase and therefore amino acid misincorporation is required for luciferase activity. Translation error was quantified by normalizing luciferase activity from in vitro translation of mutant to wild-type luciferase mRNA.

### Reconstitution of the H88 break in E. coli ribosomes

Mutant *E. coli* ribosomes were reconstituted using the iSAT system.[16] Briefly, fidelity reporter plasmids for the iSAT system were generated by mutating pk7-Luc[16] by site-directed mutagenesis to contain a missense mutation at position K529 in firefly luciferase. To introduce the H88 rRNA break into *E. coli* ribosomes, pT7rrn which encodes the *E. coli* rRNA was mutated to add 23S 3′ and 5′ processing stem sequences between 23S rRNA nucleotides 2411 and 2412 by around-the-horn PCR and ligation. 70S ribosomal proteins (TP70) and S150 cell extract were prepared as described previously.[71,72] Each iSAT reaction was performed in a final 10 μL volume and contained 3.3 μL S150 extract, 300 nM TP70 protein, 60 μg $mL^{-1}$ T7 RNA polymerase, 1 μL of 40% (v/v) PEG-8000 in a final concentration of 8 mM magnesium glutamate, 10 mM ammonium glutamate, 130 mM potassium glutamate, 0.85 mM GTP, 0.85 mM UTP, 0.85 mM CTP, 1.2 mM ATP, 34 μg $mL^{-1}$ folinic acid, 0.171 mg $mL^{-1}$ *E. coli* tRNA, 0.33 mM NAD, 0.27 mM CoA, 4 mM oxalic acid, 1 mM putrescine, 1.5 mM spermidine, 57 mM HEPES, 2 mM amino acids, 37 mM PEP, 4 ng $\mu L^{-1}$ pk7-Luc reporter wild-type or fidelity mutant plasmid, and 13.3 ng $\mu L^{-1}$ pT7rrn wild-type or H88 mutant plasmid. iSAT reactions were incubated for 8 h at 37 °C to allow for ribosome assembly and reporter expression. Either 2 μL (for wild-type pk7-Luc) or 10 μL (for fidelity mutant pk7-Luc) of the iSAT reaction were added to 30 μL ONE-Glo Luciferase assay reagent (Promega) on ice, and measured on a plate reader for 20 min at 22 °C. The maximum luminosity of this measurement was used to calculate Luc abundance in each reaction. Subsequently, RNA was isolated from iSAT reactions using a RNeasy RNA extraction kit (Qiagen). For RNA gel electrophoresis, 1 μg RNA was analyzed on a 1% agarose gel made with 1× TAE buffer, 1% bleach and 1× SYBRsafe stain.

### A-site tRNA filter binding

BsT-TyrCUA, a plasmid containing a T7 promoter followed by *B. stearothermophilus* tyrCUA gene, was used as template for synthesis of the amber suppressor tRNA.[40] The plasmids containing modified anticodon sequences were prepared by around-the-horn PCR and ligation using a shared Tyr-ATH-R primer (5′-AGTCCGCCGCGTTTAGCCACT-3′) and variant-specific forward primers (listed in key resources table). Suppressor tRNA templates for in vitro transcription were prepared by digestion of the WT and variant BsT-TyrCUA plasmids with bstNI. T7 in vitro transcription of radiolabeled suppressor tRNA was performed using final concentrations of 50 μM UTP and 0.4 μCi $\mu L^{-1}$ [α-32P]-UTP (Perkin Elmer) for radiolabeling.[73]

A plasmid containing the *ActB* 5′ UTR followed by AUG-UAG codons was prepared by amplification of the UTR sequence from HEK293T cDNA and Gibson cloning into pcDNA4 Rluc.[41] Start-stop mRNA templates were prepared by PCR using a shared T7-ActB-F primer (5′-TAATACGACTCACTATAGGG-3′) and stop-codon-specific reverse primers (listed in key resources table). Diphtheria toxin (dtA) mRNA was transcribed by T7 in vitro transcription using a template synthesized by Integrated DNA Technologies. Recombinant tyrosyl-tRNA synthetase (TyrRS) was expressed and purified from *Escherichia coli* as previously described.[73]

To charge the suppressor tRNAs, 50 μM radiolabeled suppressor tRNA, 2.5 μM TyrRS, and 1 mM 4-Benzoyl-phenylalanine (ChemImpex) were incubated in a final reaction containing 50 mM HEPES-KOH pH 7.4, 100 mM KOAc, and 1 mM MgOAc2 for 10 min at 30 °C.[74] A-site tRNA binding assays were performed using a Bio-Dot vacuum apparatus with nitrocellulose membranes

(Prometheus) and Hybond N+ membranes (Cytiva) pre-soaked in cold RB buffer (50 mM HEPES-KOH pH 7.5, 250 mM KCl, 70 mM NH4Cl, 10 mM MgCl2, 1 mM DTT). Ribosome-mRNA complexes were assembled using ribosome-depleted RRL supplemented with purified ribosomes (300 nM MNase-treated) and stalled using dtA mRNA to inhibit eEF2. A-site tRNA binding was initiated by addition of charged suppressor tRNA and measured by filter binding at indicated timepoints, washing with RB buffer, air drying, and phosphorimager imaging. For near-cognate binding assays, intensity values were normalized to parallel cognate tRNA reactions for each ribosome preparation.

### Protein aggregate isolation and quantification

For measuring native protein aggregation, frozen tissue powder was resuspended in 15× volume of fractionation buffer (20 mM Tris-HCl pH 8, 1 mM EDTA-KOH pH 8, 0.33 M sucrose)[75] and centrifuged for 5 min at 4 °C at 2000 × g. The supernatant was centrifuged for 10 min at 4 °C at 6000 × g, and the resulting supernatant was taken as a total protein sample. 1.5 mg of total protein was centrifuged for 90 min at 4 °C at 66,000 rpm in a TLA-110 rotor. The pellet, which contains microsomal membranes and aggregated proteins, was resuspended in 3 mL of fractionation buffer with 0.3% (v/v) Triton-X 100, incubated for 16 h at 4 °C with continuous shaking, and centrifuged for 60 min at 4 °C at 50,000 rpm in a TLA-110 rotor. The aggregate pellet was resuspended in fractionation buffer with 0.3% (v/v) Triton-X 100, centrifuged for 20 min at 4 °C at 16,000 × g, and resuspended in 150 μL of fractionation buffer with 0.3% (v/v) Triton-X 100 by three rounds of sonication at 25% power for 10 s using a Q700 sonicator (QSonica). Total and aggregate protein was separated by SDS-PAGE, stained with Coomassie Blue, and gel lane intensity was calculated using ImageLab.

To generate HA-tagged firefly luciferase plasmids for aggregation assays, pcDNA4 *PSMB6* 5' UTR FLuc[42] was used to generate pcDNA4 CrPV IRES HA-Fluc by Gibson cloning. RNAs containing inosine were transcribed as above but with 2.9 mM ATP and 0.1 mM ITP. In vitro translation reactions were assembled as described above but using HA-tagged firefly luciferase mRNA and incubated for 3 h at 30 °C, a timepoint chosen to obtain equivalent total levels of luciferase protein synthesized by all ribosomes. The reaction was fractionated into soluble and aggregate fractions by centrifugation for 40 min at 4 °C at 91,000 rpm in a TLA 100.4 rotor. Pelleted aggregated protein was resuspended in 10 μL of 8 M urea and incubated at 23 °C for 1 h. Soluble and aggregate protein was analyzed by immunoblot with an anti-firefly luciferase antibody (Proteintech, 27986-AP-1). Gel band intensity was calculated using ImageLab (BioRad).

### Proteasome activity assays

Frozen tissue powder was resuspended in 3× volume ice cold PBS-E (PBS with 5 mM EDTA) and homogenized by sonication at 25% power for 6 sec. Lysate was centrifuged for 5 min at 4 °C at 13,000 × g and the supernatant diluted to a final concentration of 1.3 mg $mL^{-1}$ in cold PBS-E. 50 μL of Proteasome-Glo reagent (Promega) was added, samples were incubated for 1 h at 23 °C, and proteasome activity was measured as luminescent signal intensity in a 96-well plate reader.

### Immunohistochemistry

Cephalopod arms freshly dissected from wild-caught animals or obtained from museum samples (stored in 70% ethanol) were fixed in PFA buffer (PBS with 4% (v/v) paraformaldehyde) at 4 °C for 16–24 h with rocking. Following fixation, tissues were washed with PBS and stored in 50% (w/v) sucrose at 4 °C for 48–72 h, embedded in O.C.T (Tissue-Tek, Sakura Finetech) and frozen at −80 °C for at least 24 h. Embedded tissues were sectioned using a cryostat (Leica CM3050S) at 20 μm sections. Sections were dried at room temperature for 30–60 min and stored at −20 °C overnight. After serial washes in PBST buffer (PBS with 0.3% Triton X-100), samples were blocked for 1 h in blocking buffer (PBST buffer with 5% (v/v) normal goat serum, 0.2% (w/v) bovine serum albumin) and incubated with 50 μL primary antibody solution overnight. For neuronal staining, primary antibody was a mouse monoclonal anti-acetylated tubulin (Sigma, T6793), followed by staining with a goat anti-mouse AlexaFluor555 secondary antibody (Invitrogen, A-21422) for 2–4 h at room temperature in blocking buffer. Samples were washed 3–5 times in PBST buffer, mounted in Vectashield with DAPI (Vector Laboratories, H-1200), and imaged with a Zeiss LSM900 confocal. For general tissue histology, sections were stained with hematoxylin and eosin dye (Abcam, ab245880) as per manufacturer's protocol. Protein aggregates in tissue sections were labeled using Proteostat Aggresome detection kit (Enzo Life Sciences, ENZ-51035), Nile Red staining kit (Abcam, ab228553), or Amytracker630 (Ebba Biotech) as per kit instructions.

### *Ex vivo* tissue culture

Octopus and squid arms were sedated in 15% ethanol and euthanized as per IACUC protocols. Arms were dissected in sterile artificial sea water (430 mM NaCl, 10 mM KCl, 10 mM CaCl2, 50 mM MgCl2, 10 mM HEPES, 10 mM glucose) and maintained ex vivo in a modified Leibovitz's L15 medium (ThermoFisher) adjusted to 430 mM NaCl, 10 mM KCl, 10 mM CaCl2, 50 mM MgCl2, 10 mM HEPES, 10 mM glucose, 4% FBS, 1% penicillin/streptomycin, at pH 7.8 and 980 mOSM, at 18 °C for 24 h. Pharmacological treatments of cultured arms were carried out with 2 mg $mL^{-1}$ G418 (Fisher), 10 μg $mL^{-1}$ S-MG132 (Cayman Chemical Company) or DMSO (vehicle control).

### rRNA break analysis RT-PCR

*Grimpoteuthis* tissue fragments were collected in 95% ethanol and stored in 50% ethanol until flash frozen in liquid nitrogen and ground into a fine powder using a mortar and pestle. RNA extraction was performed by mixing frozen tissue powder with 10× volume TRIzol (Invitrogen) and isolating the RNA aqueous phase according to the manufacturer's protocol. RNA was further purified using an

RNA Clean & Concentrator kit (Zymo), treated with DNAse I (Thermo Fisher) and converted into cDNA using a High-Capacity cDNA Reverse Transcription Kit (Thermo Fisher). PCR was performed using Q5 polymerase on the cDNA using primers spanning and upstream of the putative break site location (listed in key resources table). As a control, RNA isolated from *Octopus bimaculoides* tissue was subjected to the same protocol using break-spanning and upstream primers (listed in key resources table).

### RNA sequencing and bioinformatics

Tissue samples for RNA-seq were collected from animals in RNAlater and flash frozen in liquid nitrogen. RNA extraction, library prep and sequencing using HiSeq Rapid Run were performed by Azenta Life Sciences. Reads were quality filtered and trimmed using Trim Galore. Reference transcriptomes were de novo assembled using Trinity[51] and open reading frames were determined using Transdecoder. Reads were pseudo-aligned and transcript abundance was estimated using Kallisto[52] using the de novo transcriptome assembly as the reference. Annotation was performed using DIAMOND.[53] Sequencing data generated from this study are available at NCBI under BioProject: PRJNA1199547 and GEO: GSE284564.

### rDNA phylogenomics

To understand how the break site evolved in cephalopods, a BLAST search was performed against the non-redundant nucleotide database using a query sequence that was 50 bases up and downstream of the break site from *Octopus bimaculoides*. The full sequences from these queries from Genbank were downloaded using the read.genbank function in R. These sequences were aligned with MAFFT v7.490[54] using the L-INS-I algorithm. A constrained and dated phylogenetic tree was built using IQ-TREE. To constrain the topology of the tree based on prior studies, the following constraint tree was used: '(((((Eledone cirrhosa,Octopus sinensis),Grimpoteuthis sp.),Vampyroteuthis infernalis),(Euprymna morsei,Sepietta oweniana)),Nautilus pompilius).' To date the tree, dates were included from a recent phylogenomic study on mollusks.[29] The best fitting model of sequence evolution was found with ModelFinder[56] implemented in IQ-TREE, using 1000 ultrafast bootstraps to get support measures for nodes.[57] To understand whether the break site was a lineage-specific innovation in Incirrates, a sliding window analysis using 10 nucleotide windows was performed that calculated the branch length of the branch leading to Incirrate octopuses along with the average branch length across the entire cephalopod tree.

To understand conservation of this region outside of cephalopods, ribosomal RNA sequences were found in genomes by using blastn[76] with an e-value cut-off of $1\times10^{-5}$ using the *O. bimaculoides* genomic rDNA around the break site as a query. Sequences shorter than 300 nucleotides were removed and surviving sequences were clustered using cd-hit[59] (clustering threshold of 1). Sequences were aligned using MAFFT v7.490[54] using the L-INS-I algorithm, then poorly aligning sequences were removed with trimAl.[60] Consensus rDNA sequences were generated for each species using DECIPHER and used for downstream analysis.

### Inference of relaxed or intensified selection

To understand whether the H88 break had downstream effects on the evolution of protein synthesis and degradation pathway components, rates of relaxed or intensified selection were compared using RELAX.[58] Human proteins annotated with eggNOG-mapper[61] were used to identify relevant genes. Homologs across molluscan genomes were found by identifying the reciprocal best BLAST hit (e-value cut-off $10^{-10}$). Proteins were aligned using MAFFT (L-INS-I) and codon alignments were generated with PAL2NAL.[62] Octopus and squid proteins were categorized as undergoing relaxed, intensified, or no change in selection relative to background. Increases in relaxed selection were estimated using a logistic regression model on both untrimmed and trimmed codon alignments.

### Octopus depth analysis

Research-grade species distribution data for all cephalopods were downloaded from GBIF.[65] These data were categorized as Cirrate or Incirrate based on their Families.

## QUANTIFICATION AND STATISTICAL ANALYSIS

All significance tests were justified considering the experimental design and tested for normal distribution and variance using standard tests for normality. Sample sizes were chosen based on the number of independent experiments required for statistical significance and technical feasibility. All graphs and statistical analyses were performed in GraphPad Prism (GraphPad Software; RRID:SCR_002798).

Statistical comparisons between two groups were performed using unpaired Welch's t-tests to account for unequal variance between groups, as indicated in figure legends (*$p < 0.05$, **$p < 0.01$, ***$p < 0.005$, ****$p < 0.0001$). For Figure S5H, comparisons of proteasomal gene selection were performed using logistic regression as described in method details. Statistical details for each experiment (exact n values, definitions of n, and what each n represents) are provided in the figure legends. Proteasome activity data (Figure S5C) were analyzed by ANOVA followed by Welch's t-tests. Means and standard errors of the mean (s.e.m.) are shown in all graphs. All reported n values represent independent biological or experimental replicates as defined in the relevant figure legend.